

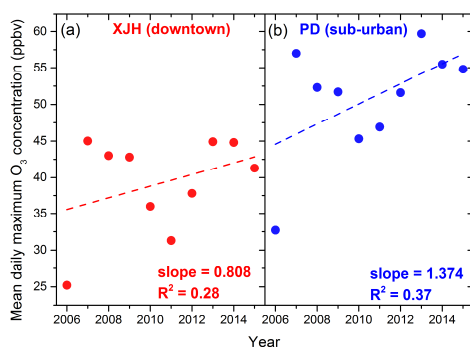
1           **Responses to Reviewer 1:**

2  
3           We thank the reviewer for the careful reading of the manuscript and helpful  
4 comments. We have revised the manuscript following the suggestions as is  
5 described below.

6  
7 (1) This manuscript apparently focused on the daytime O<sub>3</sub> formation  
8 mechanisms (VOC-limited or NO<sub>x</sub>-limited). But most of the analysis is conducted  
9 for daily mean O<sub>3</sub> concentration. Daytime O<sub>3</sub> and nighttime O<sub>3</sub> are affected by  
10 totally different processes/mechanisms and they may have different  
11 variations/trends. The trend of daily mean O<sub>3</sub> discussed mostly in this  
12 manuscript may be dominated by the trend of nighttime O<sub>3</sub>, which are not  
13 governed by the daytime O<sub>3</sub> formation mechanisms (VOC-limited or  
14 NO<sub>x</sub>-limited). Given that this manuscript wants to focus on NO<sub>x</sub>-limited or  
15 VOC-limited, I would recommend the authors change their analysis to focus on  
16 daily maximum O<sub>3</sub>.

带格式的： 字体：非加粗

17  
18           According to the excellent suggestion of the reviewer, we analyzed the  
19 variation of daily maximum O<sub>3</sub> concentration instead of daily mean O<sub>3</sub>  
20 concentration in Sect. 3.1. The new results were re-plotted in Fig. 2. It was  
21 showed that the annual variation of daily maximum O<sub>3</sub> concentration also  
22 presented significant increasing trend in XJH and PD sites which was same as  
23 that of daily mean O<sub>3</sub> concentration. The increasing rate was 0.808 ppbv.yr<sup>-1</sup> at  
24 XJH site, which was lower than that at PD site of 1.374 ppbv.yr<sup>-1</sup>. The above new  
25 results were included in the revised version. Furthermore, we calculated the  
26 variability of daily maximum 8h-O<sub>3</sub> concentration, which also exhibited the same  
27 increasing trends at the rate of 1.063 and 1.403 ppbv.yr<sup>-1</sup> at XJH and PD sites  
28 respectively.



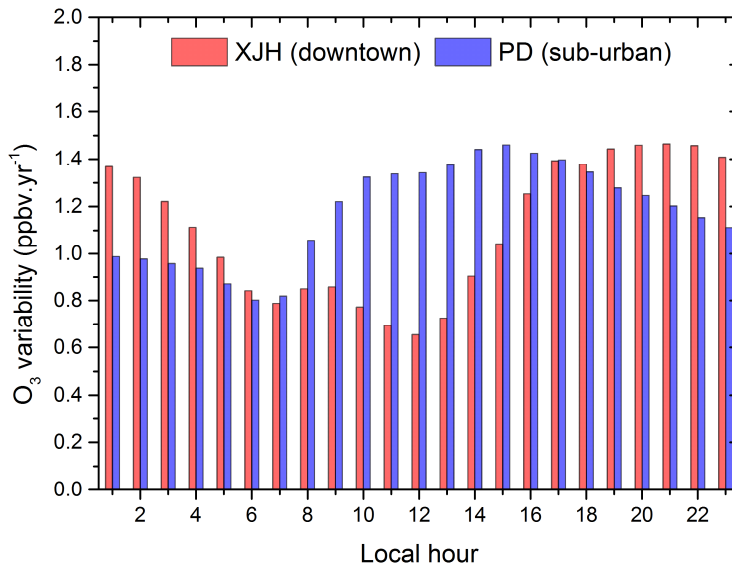
29           **Fig. 2, Annual variation of daily maximum O<sub>3</sub> concentration during 2006 to**  
30 **2015 at (a) XJH and (b) PD respectively.**

31  
32  
33 (2) Showing change of mean diurnal variation of O<sub>3</sub> would be helpful to identify  
34 the different trends of daytime/nighttime O<sub>3</sub>. In the few places when

35 daytime/nighttime O<sub>3</sub> are separately discussed in this manuscript, the time  
36 ranges for the “daytime”/“nighttime” are not specified. Thus, it is hard for this  
37 reviewer to judge whether the “daytime” O<sub>3</sub> is only affected by O<sub>3</sub> formation  
38 mechanisms or the “daytime” O<sub>3</sub> is still affected by the O<sub>3</sub> removal processes  
39 during nighttime and early morning. Thus, showing the trend of mean diurnal  
40 variation is critical.

41

42 Thanks for the reviewer's suggestion. We calculate the variability of hourly  
43 O<sub>3</sub> concentration during 2006 to 2015 to investigate the diurnal variations of O<sub>3</sub>  
44 trend in Sect. 3.4. The O<sub>3</sub> concentration showed increasing trend both in daytime  
45 (8:00-18:00, LST) and nighttime (19:00-07:00, LST) at XJH and PD sites. The  
46 nighttime O<sub>3</sub> increased more significantly than daytime O<sub>3</sub> at XJH, with the  
47 increasing rate of 1.239 and 0.956 ppbv.yr<sup>-1</sup> respectively. While at PD the O<sub>3</sub>  
48 concentration increased by 1.338 ppbv.yr<sup>-1</sup> in daytime which was higher than  
49 that in nighttime of 1.028 ppbv.yr<sup>-1</sup>. In comparison, nighttime O<sub>3</sub> presented  
50 higher increasing rate at downtown site XJH than that at sub-urban site PD due  
51 to more NO emissions at urban center or the enhanced urban effects (Hu et al.,  
52 2013). The new results were re-plotted in Fig. 6. In addition, we also compared  
53 the seasonal variability of daytime and nighttime O<sub>3</sub> concentrations at XJH. The  
54 larger O<sub>3</sub> variability in nighttime than daytime was observed in spring, summer  
55 and autumn. For example, the nighttime O<sub>3</sub> concentration increased at 1.341,  
56 1.159 and 1.525 ppbv yr<sup>-1</sup> in spring, summer and autumn respectively, which  
57 are more significant than that of 1.008, 0.378 and 1.370 ppbv yr<sup>-1</sup> in daytime.  
58 The variability of winter O<sub>3</sub> concentrations in daytime and nighttime are  
59 generally close perhaps due to the lower O<sub>3</sub> photochemical productions. The  
60 seasonal results were plotted in the Fig. 7.

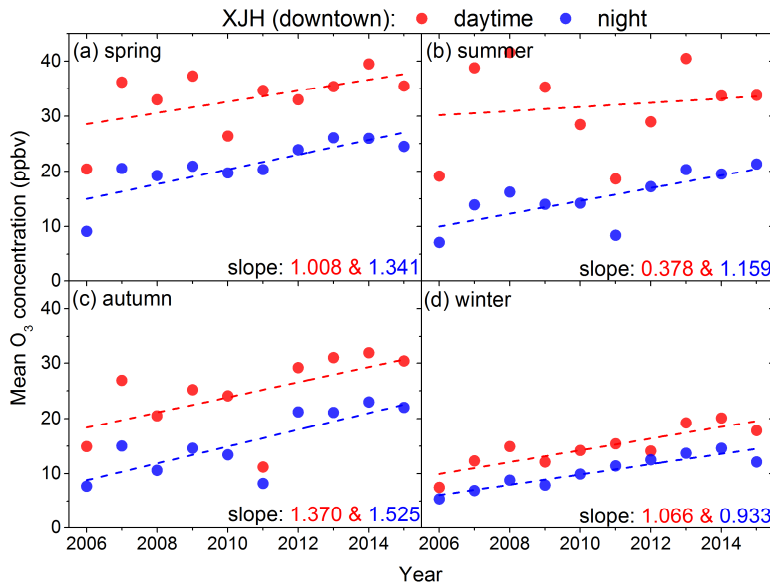


61

62

63  
64

Fig.6 The variability of hourly O<sub>3</sub> concentration during 2006 to 2015 at XJH and PD respectively



65  
66  
67  
68  
69

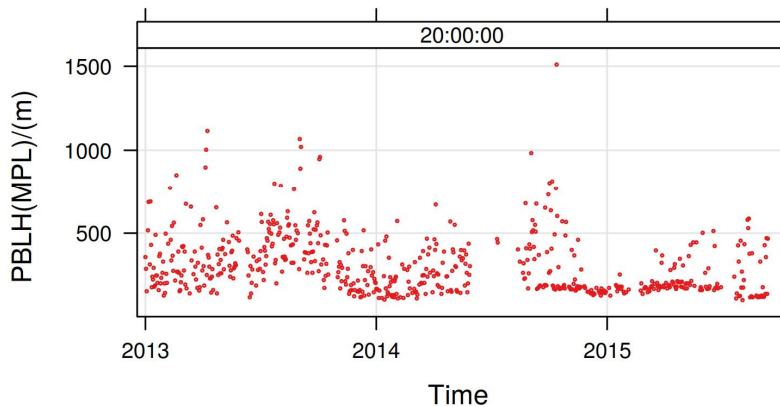
Fig.7 The variability of daytime (08:00-18:00, LST) and nighttime (19:00-07:00, LST) O<sub>3</sub> concentration during 2006 to 2015 at XJH in (a) spring, (b) summer, (c) autumn, (d) winter respectively.

70  
71  
72  
73  
74  
75  
76  
77  
78

(3) The current writing sounds like nighttime O<sub>3</sub> is only affected by NO titration. Actually nighttime O<sub>3</sub> is affected by three main processes, i.e., NO titration, dry deposition and vertical mixing (Hu et al., 2013). Both of the latter two processes are related to nighttime turbulence, which are further related to extent of urbanization. Thus the increasing trend of nighttime O<sub>3</sub> may reflect reduced NO titration, as well as enhanced nighttime vertical mixing, or say less stable nighttime boundary layer, which may be induced by enhanced urban effects through the years (Hu et al., 2016).

79  
80  
81  
82  
83  
84  
85  
86  
87  
88  
89  
90

Thank for this comment. We agreed that both dry deposition and nighttime turbulence influenced the nighttime O<sub>3</sub> concentration according to the work by Hu et al. (2013). We checked the vertical temperature gradient between 1000 hpa and 950 hpa at 20:00 (LST) in Shanghai to indicate the nighttime turbulence intensity based on sounding data, while presented no significant trend during 2010 to 2015. Furthermore, the PBL height at 20:00 (LST) retrieved from MPL measurements also varied insignificantly (slight decreasing trend) during the same period. Based on the above measurements, the variation of turbulence at night may have only minor contribution to the nighttime O<sub>3</sub> increasing in Shanghai. However the effect of dry deposition could not be excluded by lacking of measurements, which need further investigation. Such discussion has been included in Sect. 3.4.



91  
92 Fig. The retrieved PBL height at 20:00 (LST) from MPL measurements,  
93 which presented slight decreasing trend.

94  
95 Minor Comments

96 (1) LN33, in->for

97 LN48-49, I believe these should be in one sentence.

98 LN153, either remove this sentence or move it to the beginning of this  
99 paragraph.

100 LN329-342, these basic O<sub>3</sub> reactions should be put in the introduction,  
101 rather than in the results.

102 LN355-356, or more intensified urbanization in XJH (thus more  
103 enhanced downward mixing of O<sub>3</sub> (Hu, et al., 2013))

104 Thanks for the corrections, which have been revised.

105  
106 (2) anti-correlation for what time period? Nighttime anti-correlation does  
107 not indicate VOC-limited mechanism.

108 The NO<sub>x</sub> and O<sub>3</sub> measurements were strongly anti-correlated during  
109 noontime (10:00-13:00, LST), which has been revised.

110  
111 (1) LN76, what is the definition of “non-attainment days” in terms of O<sub>3</sub> in  
112 China? LN81, what is the “Chinese National Ambient Air Quality Stand” in  
113 terms of O<sub>3</sub>?

114 The "non-attainment days" of O<sub>3</sub> was defined in the ambient air quality  
115 standard (GB3095-2012) by the Ministry of Ecology and Environment of the  
116 People's Republic of China, providing the condition of daily maximum O<sub>3</sub>  
117 concentration exceeding 200 ug/m<sup>3</sup>, or daily maximum 8h-O<sub>3</sub> concentration  
118 exceeding 100 ug/m<sup>3</sup>.

119  
120 (2) LN104 “However, such O<sub>3</sub> variation responding to emission change has  
121 not been clearly investigated”. You just wrote “Gao et al. (2017) reported that O<sub>3</sub>

---

122 concentration in Shanghai downtown increased 67% from 2006 to 2015,  
123 whereas NO<sub>x</sub> concentration decreased about 38%”;

124 LN120, I thought Gao et al. analyzed 10 yr data as in this study.

125 Gao et al. (2017) has investigated the O<sub>3</sub> variation during 2006 to 2015 in  
126 Shanghai, while only limited in the downtown XJH site. In this study, we  
127 calculated and compared the variability of mean daily maximum O<sub>3</sub>  
128 concentration, and mean daily maximum 8h-O<sub>3</sub> concentration at downtown site  
129 XJH and sub-urban site PD by more comprehensive measurements. In addition,  
130 we further illustrated the O<sub>3</sub> increasing trend in the larger scale by using the O<sub>3</sub>  
131 measurements from 31 sites over Shanghai, which were not reported by Gao et  
132 al. (2017). Furthermore, this study explored the O<sub>3</sub> enhancement response to  
133 NO<sub>x</sub> reduction in Shanghai by WRF-Chem models. The effects of emission  
134 changes on long term O<sub>3</sub> variability were evaluated by WRF-Chem and compared  
135 with measurements. In addition, the shift of O<sub>3</sub> photochemical regime relative to  
136 the variations of NO<sub>x</sub> and VOCs concentrations in the past ten years was  
137 discussed by O<sub>3</sub> isopleths diagram combined with WRF-Chem to provide more  
138 insights into the O<sub>3</sub> control strategy. Moreover, the future O<sub>3</sub> levels and its  
139 possible chemical regime in Shanghai were also discussed according to the  
140 Shanghai Clean Air Action Plan. This was complemented in the part of  
141 Introduction.

142

143 (3) LN124, high-resolution? Figure 7 looks like very coarse resolution. What  
144 is the resolution in Fig. 7?

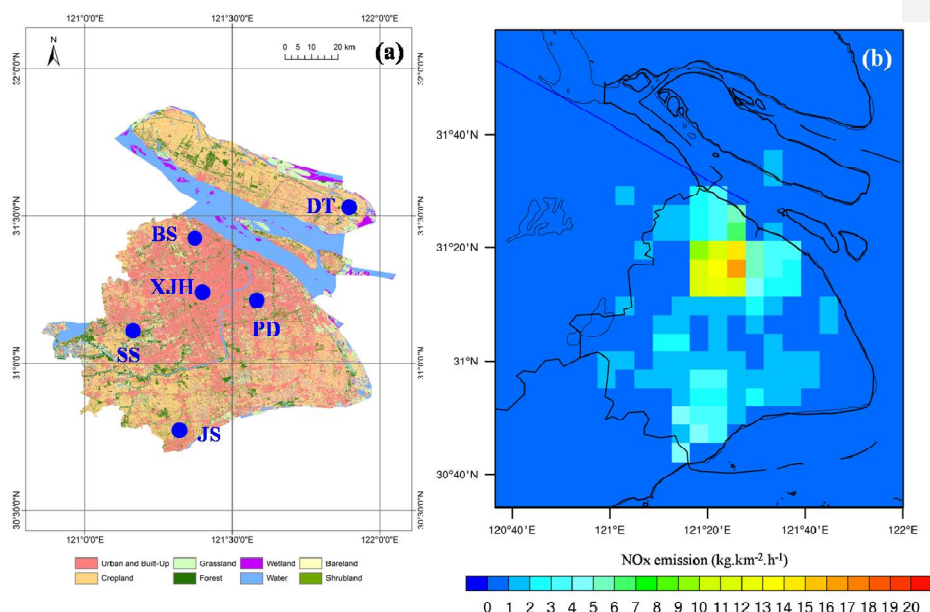
145 Fig. 7 should be combined into Fig. 1;

146 LN141-142, why these point sources do not show up on Fig. 7? Please mark  
147 these

148 major point sources in Fig. 7

149 LN204, Fig. 7 appears to have a resolution coarser than 6km.

150 The horizontal resolution set in WRF-Chem was 6km. However the emission  
151 inventory used in WRF-Chem was extracted and combined from the MEIC (0.25°)  
152 and MIRAGE-Shanghai (0.16°) emissions and equally allocated to model grids  
153 with 6 km resolution. Thus the emission in Fig.7 seemed to be a little coarse due  
154 to the coarse resolution of the emission inventory data. According to the  
155 suggestion from the reviewer, the Fig.7 was combined into Fig.1, and the major  
156 point source around BS site was marked in Fig.1.



157

158

159

160

161

162

163

164

165

166

167

168

169

170

171

172

173

174

175

176

177

178

179

180

181

182

183

Fig.1 (a) The distribution of land-use category in Shanghai. The blue dots denote the locations of 6 sites (XJH, BS, PD, SS, JS, DT), in which XJH site is located at the downtown of Shanghai, with large emission from transportation, PD site is located at the sub-urban area with the mixed emissions of transportation and residential, JS site is located in the south of Shanghai with several large chemical industries, BS site is located in the north of Shanghai with some big steel and power plants, SS site is located at the top of the sole hill (100 m a.g.l) with influence from regional transport, DT site is located at a remote island without anthropogenic activities. (b) The NO<sub>x</sub> emission of 2009 scenario in Shanghai.

(4) LN193, what aerosol module?

LN197, what is the “anon-traditional SOA module”

The WRF-Chem model used in this study was not the standard version from the WRF DOWNLOAD website. It was mainly improved by Tie et al. (2007) and Li et al. (2010; 2011). The aerosol module was developed by the US EPA (Binkowski and Roselle, 2003) and used in CMAQ model. The secondary organic aerosol (SOA) formation is simulated using a non-traditional SOA model including the volatility basis-set modeling method in which primary organic components are assumed to be semi-volatile and photochemically reactive and are distributed in logarithmically spaced volatility bins (Li et al., 2011). The partitioning of semi-volatile organic species is calculated using the algorithm suggested by Koo et al. (2003), in which the bulk gas and particle phases are in equilibrium and all condensable organics form a pseudoideal solution (Odum et al., 1996). Nine surrogate species with saturation concentrations from 10<sup>-2</sup> to 106 μgm<sup>-3</sup> at room temperature are used for the primary organic aerosol (POA) components following the approach of Shrivastava et al. (2008). The SOA

---

184 contribution from glyoxal and methylglyoxal is also included (Li et al., 2011).  
185 These were added to the revised version.

186  
187  
188 **Responses to Reviewer 2:**

189  
190 We thank the reviewer for the careful reading of the manuscript and helpful  
191 comments. We have revised the manuscript following his/her suggestions as is  
192 described below.

193  
194 (1) The manuscript analyzed the ozone concentration variation based on the  
195 measurement of 2006-2015 in Shanghai with the simulation in September 2009.  
196 Please clarify the connection between the measurement and model analyses of  
197 the ozone variation and the limitations in conclusions from modeling study.

198 First, we found the notable increasing trend of O<sub>3</sub> concentration at XJH and  
199 PD sites during 2006 to 2015 based on the long term measurements. By  
200 excluding the effects of VOCs and meteorology on the measured O<sub>3</sub> enhancement,  
201 we speculated that the O<sub>3</sub> increasing trend in Shanghai was likely attributed to  
202 the reduction of NO<sub>x</sub> concentration as a result of the strong VOCs-limited regime  
203 for O<sub>3</sub> production according to the previous studies. Then we used the  
204 WRF-Chem model to conduct sensitive experiments to demonstrate the  
205 abovementioned speculation. The simulated O<sub>3</sub> concentration increased from  
206 2009 to 2015 resulted from 30% reduction of NO<sub>x</sub> emission estimated by  
207 Shanghai Environmental Monitoring Center. The increasing rates of O<sub>3</sub> trend at  
208 downtown site XJH and sub-urban site PD were estimated by WRF-Chem model  
209 at 1.06 ppbv yr<sup>-1</sup> and 0.96 ppbv yr<sup>-1</sup>, which was very close to the observed O<sub>3</sub>  
210 growth variability. Thus we suggested that the observed increasing trend of O<sub>3</sub>  
211 concentration during the past ten years in Shanghai was mainly attributed to the  
212 reduction of NO<sub>x</sub> emission under the VOC-limited condition for O<sub>3</sub> production.

213 However there were some uncertainties and limitations existed in the study.  
214 First, in sensitive experiments the NO<sub>x</sub> emission was cut evenly for all the grids  
215 of model domain, that was to say the inhomogeneity of the NO<sub>x</sub> reduction was  
216 not considered in the sensitive experiments by lacking of the emission inventory  
217 with higher resolution. Second, the variation of VOCs emission was not taken  
218 into account due to the more uncertainties of the current inventory for VOCs.  
219 According to the studies of Geng et al. (2007, 2009), O<sub>3</sub> production in Shanghai  
220 was very sensitive to some VOC species, especially aromatics. Thus the accurate  
221 emission of VOCs need to be developed and included in the future study. Third,  
222 the same meteorology was used for all WRF-Chem experiments. However the O<sub>3</sub>  
223 photolysis, advection, and vertical diffusion were strongly affected by  
224 meteorology. For example, O<sub>3</sub> concentration in Shanghai was depressed in June  
225 due to the Meiyu period with great cloud cover inhibiting the photolysis. The  
226 summer O<sub>3</sub> concentration was mostly affected by the location and intensity of  
227 sub-tropical high which was dominant for the photochemical production. Thus

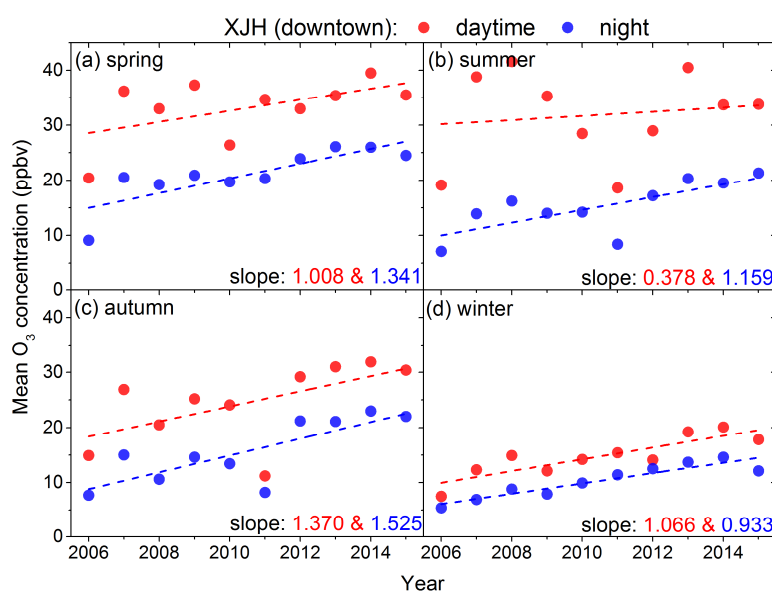
228 the variation of meteorology would be considered and evaluated in the future  
229 studies for more deep investigation. Above discussion has been complemented in  
230 the part of Conclusion.

231

232 (2) It is better to add the discussions in the measurement analyse on the  
233 interannual variations in seasonal cycle (monthly change) of daytime/ nighttime  
234 O<sub>3</sub> concentrations over 2005-2016.

235 Thanks for the suggestion. The seasonal variability of daytime and nighttime  
236 O<sub>3</sub> concentrations at XJH site were presented in the new Fig. 7. Both daytime and  
237 night O<sub>3</sub> concentrations presented increasing trends in all seasons. In  
238 comparison, the larger increasing rates of nighttime O<sub>3</sub> concentration were  
239 observed in spring, summer and autumn than that of daytime O<sub>3</sub> concentrations.  
240 For example, the nighttime O<sub>3</sub> concentrations increased at 1.341, 1.159 and  
241 1.525 ppbv yr<sup>-1</sup> in spring, summer and autumn respectively, which were more  
242 significant than that of 1.008, 0.378 and 1.370 ppbv yr<sup>-1</sup> in daytime. The  
243 variability of winter O<sub>3</sub> concentrations in daytime and nighttime were generally  
244 close perhaps due to the lower O<sub>3</sub> photochemical productions. The above results  
245 have been included in the Fig.7.

246



247

248 Fig.7 The variability of daytime and night O<sub>3</sub> concentration during 2006 to  
249 2015 at XJH in (a) spring, (b) summer, (c) autumn, (d) winter respectively.

250

251 (3) Lines 201-212: Please present the resolution of emission used in  
252 WRF-Chem modeling.

253 The emission inventory used in WRF-Chem was extracted and combined  
254 from MEIC (Zhang et al., 2009) with 0.25° resolution for the domain out of



---

255 Shanghai and the MIRAGE-shanghai (Tie et al., 2011) with 0.16° resolution for  
256 Shanghai area, which has been introduced in Sect. 2.3.

257

258 (4) Please clarify which year the meteorology is used in the modeling  
259 experiment of 2020 ozone.

260 The meteorology in September of 2009 was used for the all experiments by  
261 WRF-Chem considering that it was very close to the climatological condition in  
262 Shanghai.

263

264

265

266

---

---

267 **Measurement and model analyses of the ozone variation during 2006 to 2015 and its response**  
268 **to emission change in megacity Shanghai, China**

269 Jianming Xu<sup>1,2</sup>, Xuexi Tie<sup>3,4</sup>, Wei Gao<sup>1,2</sup>, Yanfen Lin<sup>5</sup>, and Qingyan Fu<sup>5</sup>

271  
272 <sup>1</sup> Yangtze River Delta Center for Environmental Meteorology Prediction and Warning, Shanghai  
273 Meteorological Service, Shanghai, 200135, China

274 <sup>2</sup> Shanghai Key Laboratory of Health and Meteorology, Shanghai Meteorological Service, Shanghai,  
275 200135, China

276 <sup>3</sup> Key Laboratory of Aerosol Chemistry & Physics, SKLLQG, Institute of Earth Environment, Chinese  
277 Academy of Science, Xi'an, 710061, China

278 <sup>4</sup> Center for Excellence in Urban Atmospheric Environment, Institute of Urban Environment,  
279 Chinese Academy of Science, Xiamen, 361021, China

280 <sup>5</sup> Shanghai Environmental Monitoring Center, Shanghai, 200135, China

281

282

283

284

285 Correspondence: Xuexi Tie (tiexx@ieecas.cn)

286

---

287        **Abstract.** The fine particles (PM<sub>2.5</sub>) in China decrease significantly in recent years as a result  
288 of the implement of Chinese Clean Air Action Plan since 2013, while the O<sub>3</sub> pollution is getting  
289 worse, especially in megacities such as Beijing and Shanghai. Better understanding the elevated  
290 O<sub>3</sub> pollution in Chinese megacities and its response to emission change is important for  
291 developing an effective emission control strategy in future. In this study, we analyze the  
292 significant increasing trend of daily maximum O<sub>3</sub> concentration from 2006 to 2015 in the  
293 megacity Shanghai with the variability of 0.84-1.3 ppbv yr<sup>-1</sup>. It is likely attributed to the notable  
294 reduction of NO<sub>x</sub> concentration with the decreasing rate of 1.86-2.15 ppbv yr<sup>-1</sup> accompanied with  
295 the little change of VOCs during the same period by excluding the weak trends of meteorological  
296 impacts on local dispersion (wind speed), regional transport (wind direction) and O<sub>3</sub> photolysis  
297 (solar radiation). It is further illustrated by using a state of the art regional chemical/dynamical  
298 model (WRF-Chem) to explore the O<sub>3</sub> variation response to the reduction of NO<sub>x</sub> emission in  
299 Shanghai. The control experiment conducted ~~for~~ September of 2009 shows very excellent  
300 performance for O<sub>3</sub> and NO<sub>x</sub> simulations including both the spatial distribution pattern, and the  
301 day by day variation ~~through~~ comparing with 6 in-situ measurements from MIRAGE-shanghai  
302 field campaign. Sensitive experiments with 30% reduction of NO<sub>x</sub> emission from 2009 to 2015 in  
303 Shanghai estimated by Shanghai Environmental Monitoring Center shows that the calculated O<sub>3</sub>  
304 concentrations exhibit obvious enhancement by 4-7 ppbv in urban zones with the increasing  
305 variability of 0.96-1.06 ppbv yr<sup>-1</sup>, which is well consistent with the observed O<sub>3</sub> trend as a result  
306 of the strong VOC-limited condition for O<sub>3</sub> production. The large reduction of NO<sub>x</sub> combined with  
307 less change of VOCs during the past ten years promotes the O<sub>3</sub> production in Shanghai to move  
308 towards NO<sub>x</sub>-limited regime. Further analysis of WRF-Chem experiments and O<sub>3</sub> isopleths  
309 diagram suggests that the O<sub>3</sub> production in downtown is still under VOC-limited regime after  
310 2015 despite of the remarkable NO<sub>x</sub> reduction, while moves to the transition regime between  
311 NO<sub>x</sub>-limited and VOC-limited in sub-urban zones. Supposing the insignificant VOCs variation  
312 persists, the O<sub>3</sub> concentration in downtown would keep increasing till 2020 with the further 20%  
313 reduction of NO<sub>x</sub> emission after 2015 estimated by Shanghai Clean Air Action Plan. ~~While there~~  
314 ~~are less O<sub>3</sub> change in other regions where the O<sub>3</sub> production is not under VOC limited regime.~~  
315 The O<sub>3</sub> production in Shanghai will switch from VOC-limited to NO<sub>x</sub>-limited regime after 2020  
316 except downtown area which is likely close to the transition regime. As a result the O<sub>3</sub>  
317 concentration will decrease by 2-3 ppbv in sub-urban zones, and more than 4 ppbv in suburb  
318 response to 20% reduction of NO<sub>x</sub> emission after 2020, whereas is not sensitive to both NO<sub>x</sub> and  
319 VOCs changes in downtown. This result reveals that the control strategy of O<sub>3</sub> pollution is a very  
320 complex process, and needs to be carefully studied.

321

322 **Key Words: O<sub>3</sub> pollution in Shanghai, Long-term O<sub>3</sub> trend, WRF-Chem**

323

## 324 1 Introduction

325 Ozone (O<sub>3</sub>) in the troposphere plays the important role in the oxidation of chemically and  
326 climatically relevant trace gases, hence regulating their lifetime in the atmosphere (Monks et al.,  
327 2015). In the lower troposphere, O<sub>3</sub> is produced from photochemical reactions involving volatile  
328 organic compounds (VOCs, broadly including CO) and nitrogen oxides (NO<sub>x</sub> = NO + NO<sub>2</sub>) in the  
329 presence of sunlight (Brasseur et al., 1999). As a strong oxidant, O<sub>3</sub> at ground level is detrimental  
330 to human health and vegetation (Tai et al., 2014), and has been received continuous attention  
331 from both the scientific and regulatory communities in the past three decades.

332 Shanghai has emerged as one of the largest megacities in the world over the last two  
333 decades. The city has a fleet of over 3.6 million vehicles and the population of over 2400 million  
334 permanent residents, which results in high emissions of NO<sub>x</sub>, VOCs, and primary particulate  
335 matter (PM) to the atmosphere from industrial and commercial activities, leading to the  
336 photochemical smog formation. Persistent high level of surface O<sub>3</sub> and PM were observed in  
337 Shanghai during the past ten years (Geng et al., 2007; Ran et al., 2009; Tie et al., 2009a; Xu et al.,  
338 2015). In order to mitigate the adverse impacts from severe air pollution, the Clean Air Action  
339 Plan was issued in the end of 2013 to implement the emission reduction program in Shanghai  
340 and its neighboring area. As a result, the annual mean PM<sub>2.5</sub> (particles with diameter  $\leq$  2.5  $\mu$ m)  
341 mass concentration has decreased from 50  $\mu$ g m<sup>-3</sup> in 2013 to 39  $\mu$ g m<sup>-3</sup> in 2017. However O<sub>3</sub>  
342 pollution has been continuously worsen, with the non-attainment days (daily maximum O<sub>3</sub>  
343 concentration exceeding 200  $\mu$ g m<sup>-3</sup>, or daily maximum 8h-O<sub>3</sub> concentration exceeding 100  $\mu$ g m<sup>-3</sup>)  
344 increased from 99 d in 2014 to 129 d in 2016. As a result, O<sub>3</sub> becomes the primary air pollutant  
345 affecting the ambient air quality instead of PM<sub>2.5</sub> in Shanghai. Similar issue has also been  
346 occurred in other cities in the eastern China (Lu et al., 2018). For example, the mean PM<sub>2.5</sub> mass  
347 concentration over the 74 major cities decreased by 40% from 2013 to 2017, whereas the  
348 maximum daily 8-h average O<sub>3</sub> concentration in summer exceeds the Chinese National Ambient  
349 Air Quality Standard (GB3095-2012) over most of eastern China (Li et al., 2019). Thus better  
350 understanding the causes of elevated O<sub>3</sub> in China is important for developing effective O<sub>3</sub> control  
351 strategies, especially in megacities such as Shanghai.

352 A prerequisite to an effective emission-based O<sub>3</sub> control strategy is to understand the  
353 temporal and spatial relationship between O<sub>3</sub> and its precursors, and the response of O<sub>3</sub>  
354 concentrations to the changes in emissions of O<sub>3</sub>-precursors (such as NO<sub>x</sub> and VOCs, Lin et al.,  
355 1988). The relationship of O<sub>3</sub> and O<sub>3</sub>-precursors can be clarified as NO<sub>x</sub>-limited or VOC-limited  
356 chemistry of O<sub>3</sub> formation, which is usually defined based on the relative impact of a given  
357 percent reduction in NO<sub>x</sub> relative to VOCs in the context of urban chemistry (Sillman, 1999).

358 Some observational and modeling works on O<sub>3</sub> chemical formation and transformation have  
359 been carried out in Shanghai since 2007. The O<sub>3</sub> production in Shanghai city is clearly under  
360 VOC-limited regime (Geng et al., 2007), in which the aromatics and alkenes play the dominant  
361 roles (Geng et al., 2008a). The aircraft measurements in Yangtze River Delta (YRD) region show  
362 the strong anti-correlation between NO<sub>x</sub> and O<sub>3</sub> during noontime, indicating the similar  
363 VOC-limited regime for O<sub>3</sub> production in the area neighboring Shanghai (Geng et al., 2008b). Thus  
364 either NO<sub>x</sub> reduction or VOCs growth is favorable for O<sub>3</sub> enhancement in Shanghai. Gao et al.  
365 (2017) reported that O<sub>3</sub> concentration in Shanghai downtown increased 67% from 2006 to 2015,  
366 whereas NO<sub>x</sub> concentration decreased about 38%. This is also consistent with the results of Lin et  
367 al. (2017) that, the median of the maximum daily 8-h average O<sub>3</sub> concentration in Shanghai

带格式的: 下标

带格式的: 下标

368 increased notably from 2006 to 2016, with the rate of 1.4 ppbv yr<sup>-1</sup>, while the NO<sub>2</sub> decreased  
369 from 66.7 to 42.1 μg m<sup>-3</sup> with about 20% reduction. These previous studies provide the useful  
370 information regarding the O<sub>3</sub> chemical formation and transformation in Shanghai. However, such  
371 O<sub>3</sub> variation responding to emission change has not been clearly investigated. Considering that O<sub>3</sub>  
372 formation is a complicated process including chemistry, transport, emission, deposition and their  
373 interactions, the chemical transport model is the powerful tool to gain an understanding of these  
374 interacting processes. For example, Lei et al. (2007), Ying et al. (2009) and Song et al. (2010)  
375 investigated the O<sub>3</sub> production rate and its sensitivity to emission changes of O<sub>3</sub> precursors by  
376 CAMx model in Mexico City Metropolitan Area (MCMA). Tie et al. (2013) analyzed the  
377 comprehensive data of the MIRAGE-Shanghai field campaign by WRF-Chem model, and  
378 quantified the threshold value by the emission ratio of NO<sub>x</sub>/VOCs for switching from VOC-limited  
379 to NO<sub>x</sub>-limited in Shanghai. Recently Li et al. (2019) suggested an important cause of the  
380 increasing O<sub>3</sub> in North China Plain (NCP) during 2013 to 2017 as the significant decrease in PM<sub>2.5</sub>  
381 slowing down the sink of hydroperoxy radicals and thus speeding up the O<sub>3</sub> production by  
382 GOES-CHEM model. However such implication for O<sub>3</sub> trend is not pervasive in YRD and other  
383 regions. Moreover, the 5-year O<sub>3</sub> records seem rather short to examine the inter-annual  
384 variability of O<sub>3</sub> concentration. The GOES-CHEM experiment with 50 km resolution maybe is  
385 suitable for the O<sub>3</sub> simulation at regional scale but is too coarse to resolve the local O<sub>3</sub> budget at  
386 urban scale, such as Beijing or Shanghai. To our knowledge, there are no peer-reviewed modeling  
387 studies focus on the past long term O<sub>3</sub> variations response to emission changes conducted in  
388 Shanghai. Thus this paper extends the study of Tie et al. (2013) and Gao et al. (2017) to not only  
389 further examine the inter-annual O<sub>3</sub> variations from 2005 to 2016 by long-term measurements of  
390 O<sub>3</sub> from a larger scale with more comprehensive measurements, but also explore the O<sub>3</sub>  
391 enhancement response to NO<sub>x</sub> reduction in Shanghai and predict the future O<sub>3</sub> variations by  
392 models and its precursors in Shanghai. The effects of emission changes on long term O<sub>3</sub> variability  
393 are evaluated by WRF-Chem model with high resolution and compared with measurements. The  
394 shift of O<sub>3</sub> photochemical regime relative to the variations of NO<sub>x</sub> and VOCs concentrations in the  
395 past ten years is discussed by O<sub>3</sub> isopleths diagram combined with WRF-Chem model to provide  
396 more insights into the O<sub>3</sub> control strategy. Moreover, the future O<sub>3</sub> levels and its possible  
397 chemical regime in Shanghai are also discussed according to the Shanghai Clean Air Action Plan.

398 The paper is constructed as follows. The measurements and models used for this study are  
399 described in Sect. 2. The analysis on the long-term in-situ measurements of O<sub>3</sub> and its precursors,  
400 as well as the model sensitive experiments are presented and discussed in Sect. 3-6. The  
401 conclusion is summarized in Sect. 7.

402

## 403 2 Measurements and models

### 404 2.1 Measurements

405 The measurements of O<sub>3</sub> and NO<sub>x</sub> are collected from 6 sites (XJH, PD, JS, BS, SS, DT) over  
406 Shanghai (Fig. 1 a) under different influence of air pollutant emissions. The XJH site is located at  
407 the downtown of Shanghai, which is strongly influenced by emission of transportation. The PD  
408 site is located at the sub-urban area near a big park, which is influenced by the mixed emissions  
409 of transportation and residential. The JS site is located in the south of Shanghai with several large  
410 chemical industries. The BS site is located in the north of Shanghai with some big steel and power

带格式的：下标

带格式的：下标

带格式的：下标

---

411 plants. The SS site is located at the top of the sole hill (100 m a.g.l) in Shanghai, which has minor  
412 effect from ~~regional~~ local emissions, and is influenced by regional transport. The DT site is located  
413 at a remote island without anthropogenic activities. These O<sub>3</sub> and NO<sub>x</sub> measurements are used  
414 for the evaluation on WRF-Chem performance. In addition, the VOCs are sampled at the  
415 downtown site XJH and the sub-urban site PD, and are analyzed at a chemistry laboratory. The  
416 study on the O<sub>3</sub> chemical production in this paper is limited at XJH and PD by the intensive  
417 measurements of O<sub>3</sub> and its precursors (VOCs and NO<sub>x</sub>) from 2006 to 2015 ~~at these two urban~~  
418 ~~sites~~. The meteorological measurements including wind speed and direction, solar radiation and  
419 temperature are collected at BS site, which is the only climatology observatory in Shanghai. The  
420 meteorological measurements in BS are used for international exchange of meteorological data  
421 representing Shanghai, sponsored by the World Meteorological Organization (WMO). ~~The~~  
422 ~~geographical distribution of the 6 sites is indicated in Fig. 1.~~

423

424 ~~Figure 1. (a) The distribution of topography height in Shanghai and its neighboring area. (b) The~~  
425 ~~distribution of land-use category in Shanghai. The locations of the 6 sites (XJH, BS, PD, SS, JS, DT)~~  
426 ~~are described by blue dots.~~

427

## 428 2.2 Instruments

429 O<sub>3</sub> is measured using an EC 9810 Ozone Analyzer, together with a UV photometer, which  
430 accurately and reliably measures O<sub>3</sub> concentration in ambient air. The oxides of nitrogen analyzer  
431 (EC9841B/ECOTECH) have a heated molybdenum NO<sub>2</sub> to NO converter. The resulting NO  
432 concentration is quantified using the chemiluminescence technique. This instrument has  
433 automated to set to be zero, and include an optional external valve manifold and external  
434 calibration sources. Quality control checks are performed every 3 days, including inspection of  
435 the shelter and instruments as well as zero, precision and span checks. Filter is replaced once  
436 every two weeks and calibration is made every month. The O<sub>3</sub> concentrations are recorded every  
437 1 min.

438 VOCs concentrations are sampled for 24 h every day with a 6 L silonite canister with a  
439 silonite coated valve (model 29-10622). The internal silonite coating improves long-term VOC  
440 storage. The instrument has a large volume to detect volatile chemicals down to low pptv range.  
441 Absorption is eliminated by using nupropackless valves and by eliminating teflon tape in the valve  
442 stem. These canisters are recognized to meet or exceed the technical specifications required for  
443 EP methods TO14-A and TO15. Gases samples are pre-processed using Model 7100 VOC  
444 preconcentrator. Samples are analyzed for VOCs using a gas chromatography system (Agilent  
445 GC6890) coupled with mass-selective detection (Agilent MSD5975 N) with length of 60 m,  
446 diameter of 0.32 mm, and film thickness of 1.0 μm. This measurement system can detect VOCs  
447 concentrations down to low pptv range.

448 These instruments to measure O<sub>3</sub>, NO<sub>x</sub> and VOCs concentrations are calibrated carefully.  
449 Detail information for the instruments and the procedures to perform data quality control are  
450 described by Geng et al. (2007), Ran et al. (2009), Tie et al. (2013) and Gao et al. (2017). These  
451 data have been widely used to investigate the diurnal, seasonal and inter-annual variations of O<sub>3</sub>  
452 in Shanghai (Geng et al., 2007; 2015; Tang et al., 2008; Ran et al., 2009; Gao et al., 2017) and its  
453 chemical mechanism (Geng et al., 2008a; 2008b; Tie et al., 2009a; 2013).

### 454 2.3 WRF-Chem model

455 The regional chemical/transport model (Weather Research and Forecasting Chemical model-  
456 WRF-Chem) (Grell et al., 2005) is used to investigate the O<sub>3</sub> variations response to emission  
457 changes in Shanghai. The version of the model is improved mainly by Tie et al. (2007) and Li et al.  
458 (2010; 2011). The chemical mechanism chosen in WRF-Chem is the RADM2 (Regional Acid  
459 Deposition Model, version 2) gas-phase chemical mechanism (Stockwell et al., 1990), which  
460 includes 158 reactions among 36 species. The fast radiation transfer module (FTUV) is developed  
461 and used to calculate photolysis rates (Tie et al., 2003), considering the impacts of aerosols and  
462 clouds on the photochemistry (Li et al., 2011). The aerosol modules are developed by EPA CMAQ  
463 (version 4.6) (Binkowski and Roselle, 2003). The wet deposition of chemical species is calculated  
464 using the method in the CMAQ module and the dry deposition parameterization follows Wesely  
465 et al. (1989). The ISORROPIA version 1.7 is used to calculate the inorganic aerosols (Nenes et al.,  
466 1998). The secondary organic aerosol (SOA) is predicted using a non-traditional SOA module,  
467 including the volatility basisset (VBS) modeling approach in which primary organic components  
468 are assumed to be semi-volatile and photochemically reactive and are distributed in  
469 logarithmically spaced volatility bins. The partitioning of semi-volatile organic species is  
470 calculated supposing the bulk gas and particle phases are in equilibrium and all condensable  
471 organics form a pseudoideal solution. Nine surrogate species with saturation concentrations from  
472 10<sup>-2</sup> to 10<sup>6</sup> μg m<sup>-3</sup> at room temperature are used for the primary organic aerosol (POA)  
473 components. The ~~and~~ SOA contributions from glyoxal and methylglyoxal is also included. The  
474 major physical processes employed in WRF are summarized as the Lin microphysics scheme (Lin  
475 et al., 1983), the Yonsei University (YSU) PBL scheme (Hong et al., 2006), the Noah Land surface  
476 model (Chen and Dudhia, 2001), and the long wave radiation parameterization (Dudhia, 1989).

477 The domain is set up to covered a region (centered at 32.5°N, 118°E) of 356×345 grids with  
478 a horizontal resolution of 6 km (Zhou et al., 2017). The initial and lateral boundary conditions of  
479 the meteorology are extracted from the NCEP FNL reanalysis data. The lateral meteorological  
480 boundary is updated every 6 h. The chemical lateral boundary conditions are constrained by the  
481 global chemical transport model (MOART–Model for Ozone and Related chemical Tracers) with  
482 aerosol formation modules (Tie et al., 2001; Emmonset al., 2010). Both the chemical and  
483 dynamical integration step is set as 60 s. The Multi-resolution Emission Inventory for China (MEIC)  
484 developed by Zhang et al. (2009) is used in WRF-Chem for the domain except Shanghai with 0.25°  
485 resolution. The anthropogenic emissions (including CO, NO<sub>x</sub>, SO<sub>2</sub> and VOCs) for Shanghai are  
486 developed by Tie et al. (2013) with 0.16° resolution based on the MIRAGE-shanghai field  
487 campaign. NO<sub>x</sub> and SO<sub>2</sub> emissions in YRD region are adjusted by Zhou et al. (2017) according to  
488 the performance evaluation of WRF-Chem prediction for about 195 cities during 2014–2015. The  
489 distribution of NO<sub>x</sub> emission in 2009 in Shanghai is depicted in Fig. 1b. The biogenic emissions are  
490 calculated online using the MEGAN (Model of Emissions of Gases and Aerosol from Nature)  
491 model developed by Guenther et al. (2006).

492  
493 Figure 1. (a) The distribution of land-use category in Shanghai. The blue dots denote the locations  
494 of 6 sties (XJH, BS, PD, SS, JS, DT). (b) The NO<sub>x</sub> emission of 2009 scenario in Shanghai.

### 495 2.4 OZIPR model

496 The ozone isopleths diagram for Shanghai is plot by OZIPR (Ozone Isopleths Plotting Package

带格式的：上标

带格式的：上标

带格式的：上标

带格式的：上标

带格式的：下标

带格式的：字体：加粗

带格式的：缩进：首行缩进：0 字符

带格式的：下标

497 Research) model (Gery and Crouse, 2002). The OZIPR model employs a trajectory-based air  
498 quality simulation model in conjunction with the Empirical Kinetics Modeling Approach (EKMA)  
499 to relate O<sub>3</sub> concentrations levels of organic and nitrogen oxide emissions. OZIPR simulates  
500 complex chemical and physical processes of the lower atmosphere through a trajectory model.  
501 The physical representation is a well-mixed column of air extending from the ground to the top of  
502 the mixed layer. Emissions from the surface are included as the air column passes over different  
503 emission sources, and air from above the column is mixed in as the inversion rises during the day.  
504 O<sub>3</sub> precursor concentrations and ambient information such as temperature, relative humidity and  
505 boundary layer height from measurements in Shanghai were specified for each single run.  
506 Therefore a series of simulations were performed to calculate peak O<sub>3</sub> concentration as a  
507 function of initial precursor concentrations (Tang et al., 2008; Geng et al., 2008b).

### 508 3 Variability of O<sub>3</sub> and its precursors measured in Shanghai

#### 509 3.1 Variation of O<sub>3</sub> concentration

511 Fig. 2a and b show the annual variation of daily maximum O<sub>3</sub> concentration at downtown site XJH  
512 and sub-urban site PD respectively from 2006 to 2015. The daily maximum O<sub>3</sub> concentrations  
513 increase notably during the past ten years with the increasing rate of 1.0570.808 ppbv yr<sup>-1</sup> at XJH  
514 and 1.3741.346 ppbv yr<sup>-1</sup> at PD respectively. In similar the daily maximum 8h-O<sub>3</sub> concentration  
515 also increased at the rate of 1.06 and 1.4 ppbv yr<sup>-1</sup> respectively. It is consistent with the reported  
516 O<sub>3</sub> increasing trend ranging from 1-2 ppbv yr<sup>-1</sup> at background and urban sites in eastern China  
517 during 2001 to 2015 (Tang et al., 2009; Ma et al., 2016; Sun et al., 2016). In 2006, the mean daily  
518 maximum O<sub>3</sub> concentrations at XJH and PD are 25.220 ppbv and 32.728 ppbv respectively. While  
519 in 2017, the mean daily maximum O<sub>3</sub> concentrations at the two sites increase to 41.335 ppbv and  
520 51.842 ppbv respectively, with 64.26% and 58.30% enhancement compared with that in 2006. The  
521 mean daily maximum O<sub>3</sub> concentration at downtown site XJH during 2006 to 2015 is 39.232 ppbv,  
522 which is significantly lower than that at sub-urban site PD of 50.736 ppbv, suggesting the O<sub>3</sub> is  
523 depressed in downtown area. Geng et al. (2007) suggested that the O<sub>3</sub> production in the city of  
524 Shanghai was under VOC-limited regime, thus higher NO<sub>x</sub> in downtown resulted in lower O<sub>3</sub>  
525 concentration. Considering the inhomogeneous spatial distribution of the precursors of O<sub>3</sub> in  
526 Shanghai (Geng et al. 2008a), we extend the analysis on O<sub>3</sub> variations to a broader scope by using  
527 the O<sub>3</sub> measurements from 31 sites provided by Shanghai Environmental Monitoring Center,  
528 covering the entire Shanghai area. It is shown in Fig. 2c that the median of the O<sub>3</sub>-8h  
529 concentration also increases significantly from 2006 to 2015, with the increasing rate of 1.571  
530 ppbv yr<sup>-1</sup>, indicating that the significant increasing trend of O<sub>3</sub> concentration not only occurs in  
531 the city of Shanghai, but also expanded to a larger area nearby Shanghai. Li et al. (2019) also  
532 reported a regional O<sub>3</sub> increasing phenomena in summer during 2013 to 2017 from Shanghai to  
533 Beijing in eastern China.

534 In order to analyze the individual contribution to the long-term O<sub>3</sub> trend, the variations of O<sub>3</sub>  
535 precursors, and meteorological parameters are measured and showed in the following sections.

536  
537 **Figure 2.** The ~~mean~~ annual variation of daily maximum O<sub>3</sub> concentration (ppbv) from 2006 to  
538 2015 at (a) downtown site XJH and (b) sub-urban site PD, both presenting the significant  
539 increasing trends with 1.0570.808 ppbv yr<sup>-1</sup> at XJH and 1.3461.374 ppbv yr<sup>-1</sup> at PD. The variation

带格式的：上标



---

540 of the median 8-h O<sub>3</sub> concentration (ppbv) from 2006 to 2015 averaged for 31 sites over  
541 Shanghai (c), also shows the increasing variability of 1.571 ppbv yr<sup>-1</sup>.

542

### 543 3.2 Variations of the precursors (NO<sub>x</sub> and VOCs)

544 It is well known that the tropospheric O<sub>3</sub> formation is throughout a complicated photochemical  
545 process, and is strongly related to the precursors of O<sub>3</sub> (VOCs and NO<sub>x</sub>). According to the previous  
546 studies (Geng et al., 2007; Ran et al., 2009), the chemical formation of O<sub>3</sub> in Shanghai is revealed  
547 to be under VOC-limited. Thus either enhancement of VOCs or reduction in NO<sub>x</sub> would both  
548 result in the growth of O<sub>3</sub> concentration. In order to better understanding the factors possibly  
549 driving the O<sub>3</sub> increasing trend depicted in Fig. 2, the variations of NO<sub>x</sub> and VOCs concentrations  
550 at XJH and PD in the same period are presented in Fig. 3. The NO<sub>x</sub> concentrations present  
551 significant decreasing trend from 2006 to 2015 at both XJH and PD sites, which is opposite to the  
552 increasing trend of O<sub>3</sub> variations in Fig. 2. At XJH, the decreasing rate of NO<sub>x</sub> is 2.15 ppbv yr<sup>-1</sup>,  
553 which is more remarkable than that at PD site of 1.86 ppbv yr<sup>-1</sup>. According to the studies by Lin et  
554 al (2017), the reduction of NO<sub>x</sub> concentration in Shanghai was likely attributed to the  
555 implementation of stringent emission control strategy for transportation, including improvement  
556 of gas quality, popular usage of electricity cars, and limitation of heavy cars into the urban zones.  
557 These regulations significantly decrease the emissions of NO<sub>x</sub> into the atmosphere, resulting in  
558 lower NO<sub>x</sub> concentrations. Zheng et al. (2018) also reported the 30% reduction of NO<sub>x</sub> emission in  
559 the past 5 years in YRD region. In comparison, the VOCs concentrations at XJH and PD decrease  
560 very slightly during 2006 to 2015. At XJH, the mean VOCs concentration during 2013 to 2015 is  
561 about 20 ppbv, which is some lower than that during 2009 to 2012 of 23 ppbv. At PD, the VOCs  
562 concentration shows strong inter-annual variations, ranging from 16 to 22 ppbv. Generally the  
563 VOCs concentration at the downtown site XJH is higher than that at the sub-urban site PD by 14%.  
564 It is consistent with the studies of Cai et al. (2010), suggesting that about 25% of VOCs is  
565 attributed to the vehicles in shanghai urban zones.

566

567 **Figure 3.** The mean annual concentrations (ppbv) of NO<sub>x</sub> (dots) and VOCs (bars) from 2006 to  
568 2015 at (a) downtown site XJH and (b) sub-urban site PD respectively. The NO<sub>x</sub> concentrations at  
569 XJH and PD both present obvious decreasing trends with -2.1 ppbv yr<sup>-1</sup> and -1.87 ppbv yr<sup>-1</sup>. While  
570 the VOCs concentrations at both sites present no clear inter-annual trends.

571

### 572 3.3 Meteorological impacts on O<sub>3</sub> photolysis, dispersion and transport

573 In addition to the precursors, meteorology such as solar radiation and wind speed and directions  
574 also plays the important roles in O<sub>3</sub> concentration through the photochemical and physical  
575 processes. Fig. 4 shows the annual variation of wind speed and total solar radiation from 2006 to  
576 2015. The solar radiation presents weak annual variations ranging from 140 to 150 Wm<sup>-2</sup>,  
577 exhibiting a large variability but without a significant trend. As a result, the variation of solar  
578 radiation cannot explain the significant change of O<sub>3</sub> concentration on the view of photolysis. The  
579 wind speed is usually regarded as the indicator for the dispersion capacity for air pollutants.  
580 Several studies reported that the wind speed in winter in eastern China presented decreasing  
581 variability during the past 40 years due to the decadal variation of winter monsoon affecting the

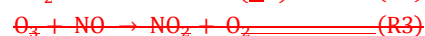
582 haze occurrence (Wang et al., 2016; Zhao et al., 2016; Xu et al., 2017). While high O<sub>3</sub> events  
 583 usually occur in summer season for middle-latitude cities such as Shanghai (Wang et al., 2017).  
 584 ~~The mean summer wind speeds in Fig. 4a show slight decreasing from 2006 to 2015, while~~  
 585 ~~without significant trends.~~The mean summer wind speed in Fig. 4a fluctuates between 3.3 ms<sup>-1</sup>  
 586 to 3.9 ms<sup>-1</sup> during 2006 to 2015 except the minimum value in 2014 (2.9 ms<sup>-1</sup>) due to fewer  
 587 typhoon in the period. Without 2014, the variability of summer wind speed is insignificant, with a  
 588 trend of -0.02 m s<sup>-1</sup> yr<sup>-1</sup>, which could not be regarded as the dominant factor to interpret the  
 589 increasing O<sub>3</sub> trend. Local O<sub>3</sub> concentration would be affected by transport of upstream plumes  
 590 usually determined by wind direction. Geng et al. (2011) suggested that O<sub>3</sub> concentration was  
 591 higher in west wind compared with other wind sectors in Shanghai indicating the possible O<sub>3</sub>  
 592 transport from western area out of Shanghai. Fig. 5 presents the annual wind rose at Baoshan  
 593 site from 2006 to 2015, presenting the very similar pattern of wind direction in each year. The  
 594 mean wind direction concentrates in the sector between 60-80 degree, suggesting the dominant  
 595 wind in Shanghai is easterly accounting for 50%. The east wind in Shanghai usually carries with  
 596 the clean air mass from the sea to improve the local air quality (Xu et al., 2015). The frequency of  
 597 west wind changes little during 2006 and 2015 ranging from 10-15%, suggesting that the regional  
 598 transport is not a major factor driving the O<sub>3</sub> increasing. Based on the above analysis, it is  
 599 speculated that the rapid O<sub>3</sub> increasing during 2006–2015 in shanghai is likely attributed to the  
 600 reduction of NO<sub>x</sub> concentration as a result of the VOC-limited condition for O<sub>3</sub> production.

601  
 602 **Figure 4.** The annual variation of (a) summer wind speed (m s<sup>-1</sup>) and (b) total solar radiation (W  
 603 m<sup>-2</sup>) from 2006 to 2015 in Shanghai. Both wind speed and the solar radiation present weak  
 604 inter-annual variations but without significant trends.

605  
 606 **Figure 5.** The wind rose in each year from 2006 to 2015 in Shanghai. The red line means the  
 607 resultant vector suggesting the dominant wind direction.

### 609 3.4 Different O<sub>3</sub> variability in nighttime and daytime

610 ~~To further qualify the changes of O<sub>3</sub>-precursors, especially NO<sub>x</sub> on the measured O<sub>3</sub>-variability,~~  
 611 ~~intensive model studies are applied. At first, a brief O<sub>3</sub>-daytime and nighttime chemistry is~~  
 612 ~~described. As we know, O<sub>3</sub> in the Earth's atmosphere is ultimately formed from the combination~~  
 613 ~~reaction of atomic oxygen (O<sup>3</sup>P) and molecular oxygen (O<sub>2</sub>) (R1). In the troposphere with little UV~~  
 614 ~~radiation, photolysis of NO<sub>2</sub> at wavelengths < 424 nm (R2) is the primary source of O<sup>3</sup>P atoms~~  
 615 ~~and prompts O<sub>3</sub>-production. Once formed, O<sub>3</sub> readily lost with reaction with NO to converts back~~  
 616 ~~to NO<sub>2</sub> (R3). The (R1-R3) reactions result in a null cycle when no other chemical species are~~  
 617 ~~involved. However, in reality, the troposphere contains alternative oxidants (i.e., HO<sub>2</sub> and RO<sub>2</sub>)~~  
 618 ~~that efficiently convert NO to NO<sub>2</sub> (R4 and R5), resulting in the accumulation of O<sub>3</sub>.~~



619 The O<sub>3</sub> chemical mechanism in daytime includes both production and loss processes. In contrast,

带格式的：缩进：首行缩进： 0 字符

620 in nighttime, the photochemical production ceases, and there mainly exists loss process for O<sub>3</sub>. In  
621 addition both dry deposition and nighttime turbulence also have the influence in the nighttime  
622 O<sub>3</sub> concentration according to the work by Hu et al. (2013). Fig. 6 shows the trends of hourly O<sub>3</sub>  
623 variations/variability in daytime and nighttime respectively from 2006 to 2015 at XJH and PD  
624 sites respectively. The O<sub>3</sub> concentrations present increasing trends both in daytime (8:00-18:00,  
625 LST) and nighttime (19:00-07:00, LST) at XJH and PD sites, which is consistent with the results in  
626 Fig. 2. The nighttime O<sub>3</sub> concentrations increase more significantly than daytime O<sub>3</sub> at XJH, with  
627 the increasing rate of 1.239 and 0.956 ppbv yr<sup>-1</sup> respectively. While at PD site the O<sub>3</sub>  
628 concentrations increase by 1.338 ppbv yr<sup>-1</sup> in daytime which is higher than that in nighttime by  
629 1.028 ppbv yr<sup>-1</sup>. In comparison, the nighttime O<sub>3</sub> concentrations exhibit higher increasing rate at  
630 downtown site XJH than that at sub-urban site PD due to more NO emissions or more intensified  
631 urbanization (Hu et al., 2013) at urban center. Both daytime and nighttime O<sub>3</sub> concentrations  
632 present significant increasing trend at two sites, which is consistent with the results in Fig. 2. It is  
633 worthy to note that O<sub>3</sub> concentration in nighttime increases more rapidly than that in daytime.  
634 For example, at XJH the nighttime O<sub>3</sub> concentration increases at the rate of 1.47 ppbv yr<sup>-1</sup> from  
635 2006 to 2015, higher than that in daytime of 0.85 ppbv yr<sup>-1</sup>. At PD, the increasing rate of O<sub>3</sub>  
636 concentration is 1.22 ppbv yr<sup>-1</sup> in nighttime, also higher than that in daytime of 0.91 ppbv yr<sup>-1</sup>.  
637 These results suggest that the reduction of NO<sub>x</sub> concentration from 2006 to 2015 has different  
638 effects on daytime and nighttime O<sub>3</sub> variations. The O<sub>3</sub> concentration in nighttime is more  
639 sensitive to NO<sub>x</sub> reduction at downtown site, resulting in less O<sub>3</sub> lost compared with that in  
640 daytime. The results in Fig. 6 also show that the increasing rate of nighttime O<sub>3</sub> in downtown site  
641 XJH is higher than that at sub-urban site PD due to the more reduction of NO<sub>x</sub> concentration in  
642 downtown area. Furthermore, the seasonal variability of daytime and nighttime O<sub>3</sub>  
643 concentrations at XJH site are illustrated in Fig. 7. Both daytime and night O<sub>3</sub> concentrations  
644 present increasing trends in all seasons. In comparison, the larger increasing rates of nighttime O<sub>3</sub>  
645 concentration are observed in spring, summer and autumn than that in daytime. For example,  
646 the nighttime O<sub>3</sub> concentrations increase at 1.341, 1.159 and 1.525 ppbv yr<sup>-1</sup> in spring, summer  
647 and autumn respectively, which are more significant than that of 1.008, 0.378 and 1.370 ppbv yr<sup>-1</sup>  
648 in daytime. The variability of winter O<sub>3</sub> concentrations in daytime and nighttime are generally  
649 close perhaps due to the lower O<sub>3</sub> photochemical productions. These results suggest that the  
650 reduction of NO<sub>x</sub> concentration from 2006 to 2015 has different effects on daytime and nighttime  
651 O<sub>3</sub> variations. The O<sub>3</sub> concentration in nighttime is more sensitive to NO<sub>x</sub> reduction, resulting in  
652 less O<sub>3</sub> lost compared with that in daytime. The results in Fig. 6 also show that the increasing rate  
653 of nighttime O<sub>3</sub> in downtown site XJH is higher than that at sub-urban site PD due to the more  
654 reduction of NO<sub>x</sub> concentration in downtown area. Hu et al. (2016) suggested that the nighttime  
655 boundary layer tended to be less stable resulted from the enhanced sensible heat flux in urban  
656 area, thus leading to more active nighttime turbulence. The sounding measurements at 20:00  
657 (LST) in Shanghai are used to calculate the vertical temperature gradient between 1000 hPa and  
658 925 hPa to indicate the intensity of nighttime turbulence, while presenting no significant trend  
659 from 2010 to 2015. Furthermore the PBL height retrieved from Lidar measurements at 20:00 (LST)  
660 presents the similar results as soundings. Based on the above measurements, the variation of  
661 turbulence at night may have only minor contribution to the nighttime O<sub>3</sub> increasing in Shanghai.  
662 However the effect of dry deposition could not be excluded by lacking of measurements, which  
663 need further investigation.

带格式的：下标

带格式的：下标

带格式的：下标

带格式的：下标

带格式的：下标

带格式的：下标

带格式的：下标

带格式的：下标

带格式的：下标

带格式的：上标

带格式的：上标

带格式的：下标

带格式的：下标

带格式的：下标

664  
665  
666  
667  
668  
669  
670  
671  
672  
673  
674  
675  
676  
677  
678  
679  
680  
681  
682  
683  
684  
685  
686  
687  
688  
689  
690  
691  
692  
693  
694  
695  
696  
697  
698  
699  
700  
701  
702  
703  
704  
705  
706

**Figure 6.** The variability of hourly O<sub>3</sub> concentration from 2006 to 2015 at downtown site XJH (red bars) and sub-urban site PD (blue bars). The annual variations of daytime and nighttime O<sub>3</sub> concentration (ppbv) from 2006 to 2015 at (a) downtown site XJH and (b) sub-urban site PD.

**Figure 7.** The daytime (8:00-18:00, LST) and nighttime (19:00-07:00, LST) O<sub>3</sub> variability from 2006 to 2015 at downtown site XJH in (a) spring, (b) summer, (c) autumn and (d) winter.

#### 4 WRF-Chem study on the O<sub>3</sub> variation response to emission change

##### 4.1 Design of the model experiments scheme

To better understand the role of NO<sub>x</sub> emission reduction in O<sub>3</sub> variation, the WRF-Chem model is utilized to calculate the changes of O<sub>3</sub> concentrations. Lin et al. (2017) suggested that the NO<sub>x</sub> emission was reduced in Shanghai in recent years resulted from the implementation of the Shanghai Clean Air Action Plan. The NO<sub>x</sub> emission in 2015 is estimated at  $33.4 \times 10^4$  ton in Shanghai, reduced significantly by 30% compared with that in 2009 of  $44.9 \times 10^4$  ton. Thus it provided the good opportunity to examine the O<sub>3</sub> variation response to the reduction of NO<sub>x</sub> emission in Shanghai. The NO<sub>x</sub> emissions in 2009 and 2015 are put into WRF-Chem model respectively to calculate the O<sub>3</sub> concentration. The other emissions (including gas and particulate matter) and meteorology used in WRF-Chem are set to be same. As a result, the difference of O<sub>3</sub> concentrations calculated by WRF-Chem is solely attributed to the change of NO<sub>x</sub> emission between 2009 and 2015, which is furthermore compared with the measurements.

The MIRAGE-shanghai field campaign was conducted in September of 2009 to explore the O<sub>3</sub> chemical formation and transformation in Shanghai (Tie et al., 2013). The mean temperature, mean wind speed and total precipitation in this month is 25 °C, 2.85 m s<sup>-1</sup> and 89.5 mm respectively, which is very close to the climatological conditions during the past ten years from 2006 to 2015, with 24.7 °C for mean temperature, 2.81 m s<sup>-1</sup> for mean wind speed, and 126 mm for total precipitation respectively. In addition, Shanghai is located at the typical sub-tropical area. The meteorology in September is characterized as the low cloud cover and rain occurrence, the slight wind speed and humidity, as well as the moderate solar radiation intensity. As suggested by Tie et al. (2013), the chemical age of O<sub>3</sub> plume in Shanghai urban area in September of 2009 was very young, indicating that the O<sub>3</sub> production was more dependent on the local emissions under such kind of meteorology, hence providing more insights into the O<sub>3</sub> chemical mechanism response to the local emission changes. We chose the meteorology in September of 2009 as the atmospheric background for the following all the sensitive experiments by WRF-Chem.

Tie et al. (2009a; 2013) highlighted that the WRF-Chem model was capable of studying the chemical and physical processes of O<sub>3</sub> in September of 2009 during the MIRAGE-Shanghai campaign. The calculated O<sub>3</sub>, NO<sub>x</sub>, VOCs and aerosols by WRF-Chem in clean and polluted episodes are fairly in agreement with the measurements except HONO, suggesting that the emission inventory in 2009 used in the model is reasonable for the Shanghai region. Moreover the VOCs emission in Shanghai is greatly improved according to the measurements from the MIRAGE-shanghai field campaign by Tie et al. (2013). Such emission from Tie et al. (2013) representing 2009 scenario is used in this study to conduct the control experiment (T1) as the

---

707 baseline to simulate the O<sub>3</sub> and NO<sub>x</sub> concentrations in September of 2009. The T1 experiment is  
708 composed of 30 model runs for each day in September of 2009. Each model run is initiated at the  
709 20:00 (LST) and performed for 52 h integrations. The first 28 h integration is regarded as model  
710 spin-up periods, the results from the later 24 h integration is captured hourly and averaged for  
711 mean daily concentration of O<sub>3</sub> and NO<sub>x</sub>. The aim of the T1 experiment is to further evaluate the  
712 reliability of the emission inventory in 2009 used in WRF-Chem by fully comparing the calculated  
713 O<sub>3</sub> and NO<sub>x</sub> concentrations with in-situ measurements of 6 sites over Shanghai.

#### 714 4.2 The NO<sub>x</sub> emission in 2009 used for base experiment

715 ~~Fig. 7 showed~~ The distribution of NO<sub>x</sub> emission of 2009 scenario (Tie et al., 2013) in Shanghai  
716 used in WRF-Chem model ~~has been showed in Fig. 1b~~. The NO<sub>x</sub> emission is mostly distributed in  
717 the urban zones, suggesting that transportation is the important source. The NO<sub>x</sub> is largely  
718 exported in downtown and two neighboring sub-urban zones in the east and north respectively.  
719 The maximum NO<sub>x</sub> emission is estimated at 16 kg hr<sup>-1</sup> km<sup>-2</sup> at downtown, compared with 2-6 kg  
720 hr<sup>-1</sup> km<sup>-2</sup> in the sub-urban area. In addition, there is a small town located in the south of Shanghai  
721 with the similar intensity of NO<sub>x</sub> emission as the sub-urban zones. The total NO<sub>x</sub> emission of 2009  
722 scenario in Shanghai (Fig. ~~71b~~) is estimated at 41.4 × 10<sup>4</sup> ton in the model, which is close to the  
723 47.8 × 10<sup>4</sup> ton suggested by Lin et al. (2017) according to the Shanghai Environmental Year Book.

724

725 ~~Figure 7. The distribution of NO<sub>x</sub> emission (kg km<sup>-2</sup> h<sup>-1</sup>) in 2009 in Shanghai.~~

726

#### 727 4.3 Performance evaluation on the base experiment

728 The mean monthly O<sub>3</sub> concentration in September 2009 is calculated by WRF-Chem and  
729 compared with measurements over 6 sites in Shanghai. It is shown in Fig. 8 that both model  
730 simulations and in-situ measurements highlight the lower O<sub>3</sub> concentration in urban zones than  
731 that in suburb. The simulated O<sub>3</sub> concentration in downtown is 22-24 ppbv, significantly lower  
732 than that at sub-urban (30-35 ppbv) and rural area (40 ppbv), which is consistent with the  
733 measurements. The measured O<sub>3</sub> concentration at downtown site XJH is 22 ppbv, lower than that  
734 at sub-urban site PD and remote site DT by 12 ppbv and 26 ppbv respectively. Geng et al. (2007)  
735 suggested that under VOC-limited regime, the lower O<sub>3</sub> concentration in downtown was resulted  
736 from the higher NO<sub>x</sub> emission, which depressed the O<sub>3</sub> production process. Under high NO<sub>x</sub>  
737 conditions, the OH radicals are lost by the reaction of NO<sub>2</sub> + OH → HNO<sub>3</sub> (Sillman, 1995). As  
738 a result, higher NO<sub>x</sub> concentration in urban area leads to lower OH concentration, which results  
739 in smaller O<sub>3</sub> production. Tang et al. (2008) also suggested that the O<sub>3</sub> concentration in Shanghai  
740 downtown was higher ~~on~~ weekends than that on weekdays due to the reduced NO<sub>x</sub>  
741 concentration. However the discrepancy is also evident between model results and  
742 measurements. For example, the modeled O<sub>3</sub> concentrations at XJH and PD are about 2-3 ppbv  
743 higher than the measurements, perhaps due to the uncertainty of NO<sub>x</sub> and VOCs emission in  
744 urban area suggested by Tie et al. (2009a). In addition, the calculated O<sub>3</sub> concentrations in the  
745 remote site DT and chemical site JS are lower than measurements by 8 and 5 ppbv respectively.  
746 The former is resulted from the overestimation of the wind speed by WRF-Chem model leading  
747 to excessive O<sub>3</sub> transport for underestimation (Zhou et al., 2017). While the latter is mainly due  
748 to the prominent underestimation of the VOCs emission in the chemical zones suggested by Tie

---

749 et al. (2009a).

750

751 **Figure 8.** The calculated distribution of O<sub>3</sub> concentration by WRF-Chem (shade) in September of  
752 2009 compared with measurements (circles) of 6 sites over Shanghai.

753

754 Fig. 9a and b show the daily variations of O<sub>3</sub> and NO<sub>x</sub> concentrations compared between  
755 WRF-Chem simulations and the in-situ measurements over 5 sites. The statistical analysis of  
756 model performance for O<sub>3</sub> and NO<sub>x</sub> is listed in Table 1 and Table 2 respectively. The calculated  
757 magnitude and daily variation of O<sub>3</sub> concentrations agree well with the measurements,  
758 suggesting that both meteorology and photochemistry are well reproduced by WRF-Chem model.  
759 For example, the Root Mean Square Error (RMSE) calculated between modeled and measured O<sub>3</sub>  
760 concentration are 7.4, 10.5, 12, 8.6, 9.2 ppbv for XJH, JS, DT, PD and BS respectively, and the  
761 difference between the simulation results and in-situ measurement is below 10%, which are very  
762 satisfactory compare with the similar works by Geng et al (2007) and Tie et al. (2013). The  
763 correlated coefficients (R) for the mean daily O<sub>3</sub> concentration range from 0.6 to 0.8 above 99%  
764 confidence over 5 sites, indicating good consistency of day by day variations between the model  
765 results and measurements. Comparably the O<sub>3</sub> concentration is best simulated by WRF-Chem at  
766 the downtown site XJH and sub-urban site PD with the lower RMSE and better R. However the  
767 discrepancy of daily O<sub>3</sub> concentration between the model and measurements is also evident. For  
768 example, a rapid change of O<sub>3</sub> concentration from 16 to 19 in September was observed over all  
769 sites, indicating it's a regional event instead of a local phenomenon. The O<sub>3</sub> concentration firstly  
770 increases significantly during 16-19 (episode-1), then sharply decreased during the later 4 days  
771 (episode-2). The similar rapid O<sub>3</sub> change in Shanghai was also reported by Tie et al. (2009a), and  
772 their explanation is that this episode was mainly related to the intensity of the sub-tropical  
773 high-pressure system on Pacific Ocean in summer. The model captures the O<sub>3</sub> variations and  
774 magnitudes during the both risen and fallen episodes very well at downtown site XJH, but  
775 substantially underestimates the increasing variability of O<sub>3</sub> concentration during episode-1 at  
776 sub-urban and rural sites by 10-15 ppbv. Geng et al. (2008a) suggested the "chemical transport of  
777 O<sub>3</sub>" from Shanghai downtown area to the distance of 18-36 km far away, which increased the O<sub>3</sub>  
778 concentration at sub-urban or rural sites. This "chemical transport of O<sub>3</sub>" is difficult to be  
779 reflected by WRF-Chem model due to the current inventory is too coarse to accurately reflect the  
780 detailed distribution and variation of NO<sub>x</sub> emission, e.g. the NO<sub>x</sub> emission from mobile source in  
781 the city. In addition, the underestimation of the O<sub>3</sub> concentration at suburb of Shanghai in  
782 summer is possibly attributed to the model bias of sea breeze simulations. Under the condition of  
783 weak sub-tropical pressure, the sea breeze develops at noontime to yield a cycling wind pattern  
784 in Shanghai, leading to the rapid accumulation of high O<sub>3</sub> concentration. The WRF-Chem usually  
785 underestimates the sea surface temperature, which tends to accelerate the sea breeze  
786 development and weak the O<sub>3</sub> trapping in the city (Tie et al., 2009a). The calculated daily NO<sub>x</sub>  
787 concentration by WRF-Chem compared with measurements are shown in Fig. 9b. Both the  
788 modeled and measured NO<sub>x</sub> concentrations at the remote site DT are very low, with the average  
789 of 1.4 and 2.9 ppbv respectively due to seldom anthropogenic emissions there. The calculated  
790 NO<sub>x</sub> concentration at XJH and PD are generally well consistent with the measurements with the  
791 excellent R of 0.8 and 0.82 and small RMSE of 6.9 and 7.5 ppbv respectively. However the NO<sub>x</sub>  
792 concentration is underestimated by WRF-Chem at sub-urban site BS in the steel zone. The

---

793 calculated NO<sub>x</sub> concentration at BS is 16.1 ppbv, which is lower than the measurements by 5 ppbv.  
794 The difference of NO<sub>x</sub> concentrations between the model and observations is generally above  
795 10%, suggesting the performance of NO<sub>x</sub> simulation is somewhat lower than that of O<sub>3</sub>. It was  
796 also reported by Tie et al. (2007; 2009b; 2013), during the evaluation of the NO<sub>x</sub> calculations by  
797 WRF-Chem in MIRAGE-Shanghai and MIRAGE-mex campaign studies. The lifetime of NO<sub>x</sub> at the  
798 surface is about 1-2 days, shorter than O<sub>3</sub>. Thus the NO<sub>x</sub> concentration is determined by the  
799 detailed emissions and dynamical factors, which need to develop the advanced inventory with  
800 higher resolution to reproduce both the spatial distributions and temporal variations of NO<sub>x</sub>  
801 emission.

802

803 **Figure 9.** The calculated mean daily concentrations (ppbv) of (a) O<sub>3</sub> and (b) NO<sub>x</sub> at 5 sites in  
804 September of 2009 by WRF-Chem (red circles) and compared with measurements (blue circles).

805

#### 806 4.4 Sensitive study on the O<sub>3</sub> variability response to the emission change

807 The T1 experiment shows the excellent performance for O<sub>3</sub> and NO<sub>x</sub> simulations, including the  
808 spatial distribution pattern, and the day by day variation and magnitude. It is indicated that the  
809 emission in 2009 scenario used in WRF-Chem is reasonable, and the model is efficient for  
810 conducting the sensitive studies on O<sub>3</sub> variation response to the emission change. In order to  
811 better understand the measured long-term trend of O<sub>3</sub> concentration during the past ten years in  
812 Shanghai and its relationship to the emission reduction, several sensitive studies are conducted in  
813 this study (Table 3). The control study of T1 is conducted based on the NO<sub>x</sub> emission in 2009  
814 scenario in Shanghai. According to the study of Lin et al. (2017), the NO<sub>x</sub> emission in 2015 in  
815 Shanghai is reduced by 30% compared with that in 2009. Thus we conduct the sensitive  
816 experiment T2 by WRF-Chem, cutting the NO<sub>x</sub> emission by 30% compared with T1, whereas  
817 keeping the other emissions and meteorology same as T1. As a result, the calculated O<sub>3</sub>  
818 difference between T1 and T2 is likely attributed to the NO<sub>x</sub> emission reduction between 2015  
819 and 2009.

820 Fig. 10a shows the distribution of the difference of O<sub>3</sub> concentration simulated by T1 and T2  
821 (T2-T1). The reduction of NO<sub>x</sub> emission has the obvious effect on the magnitude and distribution  
822 of O<sub>3</sub> concentration. The O<sub>3</sub> concentration increases notably in urban area corresponding to the  
823 higher NO<sub>x</sub> emissions in Fig. 71, ranging from 2-7 ppbv. The enhancement of O<sub>3</sub> concentration is  
824 most significant in downtown and neighboring sub-urban zones, as well as the southern town,  
825 generally more than 4 ppbv. For example, the maximum increase in O<sub>3</sub> concentration is 6.4 ppbv  
826 occurred at downtown site XJH, followed by 4-5 ppbv at sub-urban site PD. The increasing rates  
827 of O<sub>3</sub> trend at XJH and PD are estimated at 1.06 ppbv yr<sup>-1</sup> and 0.96 ppbv yr<sup>-1</sup> from 2009 to 2015  
828 by WRF-Chem, which is consistent to the observed O<sub>3</sub> growth variability (Fig. 2) of 1-1.3 ppbv yr<sup>-1</sup>.  
829 The response of O<sub>3</sub> concentration to the NO<sub>x</sub> reduction is not evident in the rural area including  
830 the eastern part of Shanghai and the island with low NO<sub>x</sub> emissions. The comparison of T1 and T2  
831 further illustrates the speculation that the significant increasing trend of O<sub>3</sub> concentration during  
832 the past ten years in Shanghai is mostly attributed to the reduction of NO<sub>x</sub> emission as a result of  
833 the implementation of Shanghai Clean Air Action Plan.

834 The O<sub>3</sub> chemical formation is strongly related to NO<sub>x</sub> and VOCs concentrations. As discussed  
835 by Geng et al. (2008a) the O<sub>3</sub> chemical formation is clearly under VOC-limited regime in Shanghai

---

836 and its neighboring area. Under the high NO<sub>x</sub> condition, NO tends to react with O<sub>3</sub> instead of NO<sub>2</sub>,  
837 flowing by NO<sub>2</sub> + OH → HNO<sub>3</sub>, causing the decrease of the reactivity and ensuing O<sub>3</sub>  
838 concentrations. Thus reduced NO<sub>x</sub> emission would result in increase in O<sub>3</sub> concentration, which  
839 has been discussed in Fig. 10a.

840 Despite of minor change of VOCs in the last ten years, it is worth to investigate the effect of  
841 the VOCs changes on O<sub>3</sub> concentrations in Shanghai. For this purpose, we conduct a sensitive  
842 study (T3), with 50% increase of VOCs emission compared with T1, but keeping NO<sub>x</sub> and other  
843 emissions as well as the meteorology same as T1. For RADM2 gas mechanism used in WRF-Chem,  
844 the VOCs are surrogated into 14 species, such as alkane, alkene, aromatic, formaldehyde, etc. All  
845 the species of VOCs are increased by 50% at every model grid over Shanghai and at every hour.  
846 The difference of O<sub>3</sub> concentration between T3 and T1 (T3-T1) is shown in Fig. 10b. As we  
847 expected, the O<sub>3</sub> concentration in Shanghai is sensitive to the enhancement of VOCs emission,  
848 increased by 3-4 ppbv in urban area due to more NO is converted to NO<sub>2</sub> by reaction with RO<sub>2</sub>  
849 and HO<sub>2</sub>. Furthermore, the abundant O<sub>3</sub> plumes produced in the urban zones significantly  
850 transport to the downwind areas about 100-200 km away, resulting in elevated O<sub>3</sub> concentration  
851 in the western Shanghai by about 2 ppbv. According to Tie et al. (2013), the O<sub>3</sub> plume released in  
852 Shanghai urban area can be transported to downwind of the city by about 100-150 km away in  
853 the MIRAGE-shanghai field campaign. The model studies of T1, T2 and T3 highlight that under the  
854 emission of 2009 scenario, the O<sub>3</sub> chemical production is clearly under VOC-limit regime, either  
855 decreasing NO<sub>x</sub> concentration or increasing VOCs concentration would result in the O<sub>3</sub>  
856 enhancement. The analysis on in-situ measurements and model experiments jointly suggests that  
857 the significant O<sub>3</sub> increasing trend during the past ten years in Shanghai is mainly attributed to  
858 the large reduction of NO<sub>x</sub> emission.

859

860 **Figure 10.** The difference of O<sub>3</sub> concentration (ppbv) between (a) T2 and T1 (T2-T1), (b) T3 and  
861 T1 (T3-T1) respectively conducted by WRF-Chem model. The difference between T2 and T1 lies in  
862 the NO<sub>x</sub> emissions set in T2 (2015 scenario) is 30% lower than that in T1 (2009 scenario), which is  
863 estimated by Lin et al. (2017) according to the Shanghai Environment Yearbook. The difference  
864 between T3 and T1 is dependent on that the VOCs emission in T3 is 50% higher than that in T1.  
865

866

#### 866 4.5 The variation of O<sub>3</sub> production regime response to emission change

867 The O<sub>3</sub> chemical mechanism in Shanghai was explored by several studies based on the in-situ  
868 measurements around 2008 and 2009. Geng et al. (2008a; 2008b), Ran et al. (2009) and Tie et al.  
869 (2009a) all revealed that the O<sub>3</sub> production around 2008 and 2009 in Shanghai was clearly under  
870 VOC-limit regime which was further illustrated by the above model studies. As indicated in Fig. 3,  
871 the significant decrease of NO<sub>x</sub> concentration is observed from 2009 to 2015 in Shanghai, while  
872 the VOCs concentration changed little during the same period. As we know, the O<sub>3</sub> chemical  
873 formation is strongly related to NO<sub>x</sub> and VOCs concentrations with nonlinearity. Thus the  
874 different variability of NO<sub>x</sub> and VOCs concentration from 2009 to 2015 inevitably has the large  
875 effect on the O<sub>3</sub> production regime, which need to be investigated deeply.

876 The complex relationship among NO<sub>x</sub>, VOCs and O<sub>3</sub> concentrations is usually depicted by O<sub>3</sub>  
877 isopleths diagram. The O<sub>3</sub> isopleths plot (Fig. 11) in Shanghai used in this study is constructed by  
878 the OZIPR model based on the in-situ measurements of O<sub>3</sub>, NO<sub>x</sub>, VOCs and meteorology. Under



---

879 high VOCs and low NO<sub>x</sub> condition (low NO<sub>x</sub>/VOCs ratio), the O<sub>3</sub> production is not sensitive to  
880 VOCs, while positively correlated to NO<sub>x</sub> concentration, which is viewed as NO<sub>x</sub>-limited regime. By  
881 contrast, under low VOCs and high NO<sub>x</sub> condition (high NO<sub>x</sub>/VOCs ratio), the O<sub>3</sub> production tends  
882 to increase with the VOCs growth or NO<sub>x</sub> reduction, which is regarded as VOC-limited regime. The  
883 NO<sub>x</sub>-limited and VOC-limited regime is divided by a ridge line (the dot-dash line in Fig. 11) in the  
884 O<sub>3</sub> isopleths plot. The O<sub>3</sub> production is not sensitive to neither NO<sub>x</sub> concentration nor VOCs  
885 concentration when near the ridge line, which is regarded as the transition regime.

886 The O<sub>3</sub> chemical production regime at XJH and PD in 2009 and 2015 is positioned  
887 respectively in Fig. 11. In 2009 the O<sub>3</sub> production at both XJH and PD sites (marked as red and  
888 blue hollow circle respectively) are clearly under VOC-limited regime. Thus decrease in NO<sub>x</sub>  
889 concentration leads to the O<sub>3</sub> enhancement, which is highlighted by the previous in-situ  
890 measurements and model experiments. Since then the O<sub>3</sub> production regime tends to move  
891 toward the dot-dash line due to the significant reduction of NO<sub>x</sub> concentration accompanied with  
892 the relative less change of VOCs at the two sites. In 2015 the O<sub>3</sub> production at XJH (marked as red  
893 solid circle) is still under VOC-limited regime, but for PD (marked as blue solid circle), it is close to  
894 the dot-dash line, approaching the transition regime between VOC-limited to NO<sub>x</sub>-limited. This  
895 result suggests that if the NO<sub>x</sub> emission keeps reduction after 2015 assuming the VOCs  
896 concentration keeps constant, the O<sub>3</sub> concentration will continue to increase at XJH, while at PD  
897 the O<sub>3</sub> concentration is supposed to be insensitive to the NO<sub>x</sub> change. According to the O<sub>3</sub>  
898 chemical regime depicted in Fig. 11, if the NO<sub>x</sub> concentration decreases by 5 ppbv after 2015, the  
899 peak O<sub>3</sub> concentration at XJH will further increase by 3 ppbv, whereas at PD it seems to change  
900 very slightly. To better understand this further change, more sensitive studies of WRF-Chem are  
901 conducted in the following sections.

902

903 **Figure 11.** The O<sub>3</sub> chemical production at downtown site XJH and sub-urban site PD in 2009 and  
904 2015 depicted by O<sub>3</sub> isopleths diagram. The hollow and solid red circles denote O<sub>3</sub> production  
905 regime at XJH in 2005 and 2019 respectively. The hollow and solid blue circles denote O<sub>3</sub>  
906 production regime at PD in 2005 and 2019 respectively

907

## 908 **5 The future O<sub>3</sub> evaluation**

### 909 **5.1 The O<sub>3</sub> level in 2020**

910 According to the Shanghai Clean Air Action Plan, the NO<sub>x</sub> emission in Shanghai will be further  
911 reduced by 20% in 2020 compared with that in 2015. According to the above analysis based on  
912 the O<sub>3</sub> isopleths plot (Fig. 11), the O<sub>3</sub> concentrations in downtown and sub-urban seem to have  
913 distinct different responses to further NO<sub>x</sub> reduction after 2015. In order to better understand  
914 the future O<sub>3</sub> variation, the sensitive experiment T4 is conducted by WRF-Chem with 20%  
915 reduction of NO<sub>x</sub> emission compared with T2. T2 and T4 represent the NO<sub>x</sub> emission in 2015 and  
916 2020 respectively. The other emissions and meteorology are set to be same as T1. The difference  
917 of O<sub>3</sub> concentration between T2 and T4 (T4-T2) is presented in Fig. 12a. The O<sub>3</sub> concentration  
918 keeps increasing in downtown area such as XJH site, ranging from 2-4 ppbv. However, for the  
919 sub-urban zones such as the PD site, the O<sub>3</sub> concentration changes very little response to the  
920 further NO<sub>x</sub> reduction, ranging from 0-1 ppbv. As discussed in Fig. 11, in 2015 the O<sub>3</sub> production  
921 at PD is possibly under the transition regime from VOC-limited to NO<sub>x</sub>-limited near the ridge line.

---

922 As a result, the O<sub>3</sub> concentration is not sensitive to the variation of NO<sub>x</sub> concentration. However  
923 the O<sub>3</sub> concentration in the suburb zones generally decreases by 1ppbv, indicating that with the  
924 further NO<sub>x</sub> reduction after 2015 the O<sub>3</sub> chemical production transfers from VOCs-limited to  
925 NO<sub>x</sub>-limited regime in the rural of Shanghai.

926 It is suggested in Fig.11 that the O<sub>3</sub> production at downtown site XJH in 2015 is still under  
927 VOC-limited regime despite of the significant NO<sub>x</sub> reduction. The O<sub>3</sub> concentration would be also  
928 sensitive to the variation of VOCs concentration. Thus the sensitive experiment T5 is conducted  
929 by WRF-Chem model with 50% enhancement of VOCs emission compared with T2 (representing  
930 the emission in 2015 scenario). It is presented in Fig. 12b that the O<sub>3</sub> concentration increases by  
931 2-3 ppbv in downtown area due to the enhancement of VOCs, suggesting that the O<sub>3</sub> production  
932 at downtown in 2015 is still under VOC-limited regime, which is consistent with the results in Fig.  
933 11. Moreover the O<sub>3</sub> plumes produced in urban area transport to the downwind area to  
934 accumulate the high O<sub>3</sub> concentration in the western area to Shanghai by 2 ppbv. While at  
935 sub-urban site PD, the O<sub>3</sub> concentration changes less than 1 ppbv response to the increase in  
936 VOCs emission, which is similar as the very weak O<sub>3</sub> variations relative to the NO<sub>x</sub> reduction in Fig.  
937 12a. Overall, the models studies of T4 and T5 jointly suggest that the O<sub>3</sub> concentration at  
938 sub-urban site PD in 2015 is not sensitive to either NO<sub>x</sub> or VOCs variations due to the O<sub>3</sub>  
939 production is under the transition regime depicted in the O<sub>3</sub> isopleths plot.

940

941 **Figure 12.** The difference of O<sub>3</sub> concentration (ppbv) between (a) T4 and T2 (T4-T2), (b) T5 and  
942 T2 (T5-T2) respectively conducted by WRF-Chem model. The difference between T4 and T2 is  
943 that the NO<sub>x</sub> emissions set in T4 (2020 scenario) is 20% lower than that in T2 (2015 scenario),  
944 which is estimated according to the Shanghai Clean Air Action Plan. The difference between T5  
945 and T2 lies in that the VOCs emission in T5 is 50% higher than that in T2.

946

## 947 5.2 The O<sub>3</sub> chemical production after 2020

948 The above study shows that the O<sub>3</sub> production at sub-urban site PD in 2020 will likely transfer  
949 from VOCs-limited regime to NO<sub>x</sub>-limited regime without consideration of possible VOCs changes.  
950 For the purpose of the O<sub>3</sub> pollution control strategy, it is worth to estimate the O<sub>3</sub> level response  
951 to emission change after 2020 in Shanghai. It is also essential to access how many NO<sub>x</sub> emission  
952 need to be cut after 2020 will cease the O<sub>3</sub> enhancement in downtown area. Thus the sensitive  
953 experiment T6 is conducted by further 20% reduction of NO<sub>x</sub> emission from 2020 scenario (T4).  
954 The difference of O<sub>3</sub> concentration between T6 and T4 (T6-T4) is shown in Fig. 13a. It is clear that  
955 the O<sub>3</sub> concentration at downtown keeps nearly constant regardless of the further reduction of  
956 NO<sub>x</sub> emission after 2020. That is to say the increasing trend of O<sub>3</sub> in downtown with the NO<sub>x</sub>  
957 reduction ceases after 2020, indicating that the O<sub>3</sub> production likely approaches the transition  
958 regime. In addition, the O<sub>3</sub> concentration decreases significantly out of the downtown area,  
959 ranging from 2-3 ppbv in sub-urban zones, and more than 4 ppbv in suburb, indicating that the  
960 O<sub>3</sub> production in Shanghai transfers to NO<sub>x</sub>-limited regime after 2020 except the downtown area  
961 where the O<sub>3</sub> production is likely near the transition zone. On the other hand, if the NO<sub>x</sub> emission  
962 is kept constant after 2020 as T4, while the VOCs emission is increased by 50% conducted in T7  
963 experiment, the O<sub>3</sub> concentration (Fig. 13b) changes little in both urban and suburb area in  
964 Shanghai which is different from the previous model study of T5 the T3 when O<sub>3</sub> production is

965 under VOC-limited condition. It is suggested that the O<sub>3</sub> concentration after 2020 is not sensitive  
966 to the variation of VOCs concentration because the continuous reduction of NO<sub>x</sub> emission keeps  
967 in promoting the O<sub>3</sub> production to transfer into NO<sub>x</sub>-limited regime. Thus further reduction of  
968 NO<sub>x</sub> tends to decrease the O<sub>3</sub> concentration in Shanghai.

969

970 **Figure 13.** The difference of O<sub>3</sub> concentration (ppbv) between (a) T6 and T4 (T6-T4), (b) T7 and  
971 T4 (T7-T4) respectively conducted by WRF-Chem model. The NO<sub>x</sub> emissions set in T6 is 20% lower  
972 than that in T4 (2020 scenario). The VOCs emission in T7 is 50% higher than that in T4.

973

#### 974 **Conclusions**

975 O<sub>3</sub> pollution is a serious issue in China. Better understanding the elevated O<sub>3</sub> and its response to  
976 emission change is important for Chinese megacities. In this study, we analyze the increasing  
977 trend of O<sub>3</sub> concentration by long-term measurements of O<sub>3</sub> and its precursors as well as  
978 meteorology in Shanghai combined with the WRF-Chem model. The O<sub>3</sub> production regime  
979 response to the emission change in Shanghai during the past ten years is also explored by O<sub>3</sub>  
980 isopleths plot. In addition, the future O<sub>3</sub> variation and its chemical production in Shanghai are  
981 evaluated by WRF-Chem model. The main conclusions are summarized as follows:

982 (1) The daily maximum O<sub>3</sub> concentration measured in Shanghai increased significantly from  
983 2006 to 2015 with the rate of 1.0570.808 ppbv yr<sup>-1</sup> at downtown site XJH and 1.3461.374 ppbv  
984 yr<sup>-1</sup> at sub-urban site PD respectively. The observed increasing trend of O<sub>3</sub> is not limited in the  
985 urban zones but expanded to the larger scale covering the total Shanghai city. The NO<sub>x</sub> and VOCs  
986 concentrations presented different variability from O<sub>3</sub> during the same period, in which NO<sub>x</sub>  
987 concentration decreases significantly at both XJH and PD sites, whereas the VOCs changes very  
988 little without evident trend.

989 (2) Because there are minor trends of measured O<sub>3</sub> photolysis, local dispersion and regional  
990 transport resulted from meteorology, it is speculated that the significant O<sub>3</sub> increasing trend  
991 during 2006 to 2015 in Shanghai is likely attributed to the reduction of NO<sub>x</sub> concentration as a  
992 result of the strong VOCs-limited regime for O<sub>3</sub> production. The nighttime O<sub>3</sub> is more sensitive to  
993 NO<sub>x</sub> reduction than that in daytime, because of more O<sub>3</sub> is depressed by NO<sub>x</sub> in nighttime. As a  
994 result, the observed nighttime O<sub>3</sub> concentration at XJH ~~and PD~~ increases more rapidly than that  
995 in daytime response to the NO<sub>x</sub> reduction.

996 (3) The WRF-Chem model is utilized to calculate the long term O<sub>3</sub> variations response to  
997 emission change. The sensitive experiments illustrate that either reduction of NO<sub>x</sub> emission or  
998 growth of VOCs emission conducted by WRF-Chem lead to the significant enhancement in O<sub>3</sub>  
999 concentration in urban zones in 2009 as the baseline, indicating the O<sub>3</sub> production is clearly  
1000 under VOC-limited regime. The calculated O<sub>3</sub> concentration increases by 1-7 ppbv in urban zones  
1001 from 2009 to 2015 resulted from 30% reduction of NO<sub>x</sub> emission estimated by Shanghai  
1002 Environmental Monitoring Center. The enhancement of O<sub>3</sub> concentration is significant in urban  
1003 zones generally more than 4 ppbv, with the maximum elevation of 6-7 ppbv occurred at  
1004 downtown area, which is consistent with the measurements. The increasing rates of O<sub>3</sub> trend at  
1005 downtown site XJH and sub-urban site PD are estimated at 1.06 ppbv yr<sup>-1</sup> and 0.96 ppbv yr<sup>-1</sup> from  
1006 2009 to 2015 by WRF-Chem, which is close to the observed O<sub>3</sub> growth variability of 1-1.3 ppbv  
1007 yr<sup>-1</sup>. This result suggests that the observed increasing trend of O<sub>3</sub> concentration during the past  
1008 ten years in Shanghai is likely attributed to the reduction of NO<sub>x</sub> emission under the VOC-limited

1009 condition for O<sub>3</sub> production.

1010 (4) The model sensitive study suggests that significant decrease in NO<sub>x</sub> concentration  
1011 combined with the obscure VOCs variation from 2006 to 2015 gradually promotes the O<sub>3</sub>  
1012 chemical production in Shanghai from VOC-limited to NO<sub>x</sub>-limited, which is consistent with the O<sub>3</sub>  
1013 isopleths diagram. The O<sub>3</sub> isopleths plot shows that O<sub>3</sub> production is in VOC-limited regime in  
1014 both downtown site XJH and sub-urban site PD in 2009. With the 30% reduction of NO<sub>x</sub> emission  
1015 from 2009 to 2015 estimated by Shanghai Environmental Monitoring Center, the O<sub>3</sub> production in  
1016 XJH is still under VOC-limited regime, while the O<sub>3</sub> production moves to the transition regime in  
1017 PD, suggesting that the O<sub>3</sub> concentration in sub-urban zones is not sensitive to the variation of  
1018 either NO<sub>x</sub> or VOCs concentration.

1019 (5) In order to better understand the O<sub>3</sub> control strategy in Shanghai, the future O<sub>3</sub>  
1020 production is estimated by WRF-Chem. The O<sub>3</sub> concentration in Shanghai downtown would keep  
1021 increasing till 2020 with the 20% reduction of NO<sub>x</sub> emission after 2015 estimated by Shanghai  
1022 Clean Air Action Plan. If the NO<sub>x</sub> emission is further decreased by 20% after 2020, The O<sub>3</sub>  
1023 concentration will decrease by 2-3 ppbv in sub-urban zones, and more than 4 ppbv in suburb.  
1024 While the O<sub>3</sub> concentration in downtown is not sensitive to either NO<sub>x</sub> reduction or VOCs  
1025 enhancement after 2020, indicating the O<sub>3</sub> production in shanghai will transfer to NO<sub>x</sub>-limited  
1026 regimes except downtown where the O<sub>3</sub> production is likely close to the transition regime.  
1027 Further reduction of NO<sub>x</sub> emission after 2020 tend to mitigate the O<sub>3</sub> pollution in Shanghai.

1028 (6) There are some uncertainties and limitations existed in the study. First, the  
1029 inhomogeneity of the NO<sub>x</sub> reduction is not considered in the sensitive experiments by lacking of  
1030 the high resolutional emission inventory (e.g. 1 km resolution). Second, the variation of VOCs  
1031 emission is not taken into account in the model experiments due to the more uncertainties  
1032 existed in the current VOCs emission inventory. While O<sub>3</sub> production in Shanghai is very sensitive  
1033 to some VOC species, especially aromatics. Thus the accurate emission inventory of VOCs need to  
1034 be developed and included in the future study. Third, the same meteorology is used for all  
1035 WRF-Chem simulations. However the O<sub>3</sub> photolysis, advection, and vertical diffusion are all  
1036 strongly affected by meteorology. The change of meteorology would be considered and  
1037 evaluated in the future studies for more deep investigation.

带格式的：下标

带格式的：下标

带格式的：下标

1038  
1039  
1040 **Data availability.** The data used in this paper can be provided upon request from Jianming Xu  
1041 (metxujm@163.com).

1042  
1043 **Author contributions.** XT came up with the original idea of investigating the impact of emission  
1044 change on long term O<sub>3</sub> variations by. XT and JX designed the analysis method. JX conducted the  
1045 analysis. WG, YL and QF provided the observational data and helped in discussion.

1046  
1047 **Competing interests.** The authors declare that they have no conflict of interest.

1048  
1049 **Acknowledgements.** This study was funded by the National Key R&D Program of China (grant  
1050 2018YFC0213800), the National Natural Science Foundation of China (91644223, 41430424 and  
1051 41730108).

1052

---

1053 **References**

- 1054 Binkowski, F. S. and Roselle, S. J.: Models-3 community multi scale air quality (CMAQ) model  
1055 aerosol component – 1. Model description, *Journal of Geophysical Research*, 108 (D6),  
1056 4183, doi:10.1029/2001jd001409, 2003.
- 1057 Brasseur, G. P., Orlando, J. J., and Tyndall, G. S.: *Atmospheric chemistry and global change*, Oxford  
1058 University Press, Cambridge, USA, 654 pp., 1999.
- 1059 Cai, C. J., Geng, F. H., Tie, X. X., Yu, Q., and An J. L.: Characteristics and source apportionment of  
1060 VOCs measured in Shanghai, China, *Atmospheric Environment*, 44, 5005-5014, 2010.
- 1061 Chen, F. and Dudhia, J.: Coupling an advanced land surface hydrology model with the Penn  
1062 State-NCAR MM5 modeling system, Part I: Model implementation and sensitivity, *Monthly*  
1063 *Weather Review*, 129, 569–585, 2001.
- 1064 Dudhia, J.: Numerical study of convection observed during the winter monsoon experiment using  
1065 a mesoscale two-dimensional model, *Journal of the Atmospheric Sciences*, 46, 3077–3107,  
1066 1989.
- 1067 Emmons, L. K., Walters, S., Hess, P. G., Lamarque, J. F., Pfister, G. G., Fillmore, D., Granier, C.,  
1068 Aguenther, A., Kinnison, D., Laepple, T., Orlando, J., Tie, X., Tyndall, G., Wiedinmyer, C.,  
1069 Baughcum, S. L., and Kloster, S.: Description and evaluation of the model for ozone and  
1070 related chemical tracers, version4 (MOZART-4), *Geoscientific Model Development*, 3, 43–67,  
1071 2010.
- 1072 Gao, W., Tie, X. X., Xu, J. M., Huang, R. J., Mao, X. Q., Zhou, G. Q., and Chang, L. Y.: Long-term  
1073 trend of O<sub>3</sub> in a mega City (Shanghai), China: Characteristics, causes, and interactions with  
1074 precursors, *Science of the Total Environment*, 603-604, 425-433, 2017.
- 1075 Geng, F. H., Zhao, C. S., Tang, X., Lu, G. L., and Tie, X. X.: Analysis of ozone and VOCs measured in  
1076 Shanghai: a case study, *Atmospheric Environment*, 41, 989–1001, 2007.
- 1077 Geng, F. H., Tie, X., Xu, J., Zhou, G., Peng, L., Gao, W., Tang, X., Zhao, C.: Characterizations of ozone,  
1078 NO<sub>x</sub>, and VOCs measured in Shanghai, China, *Atmospheric Environment*, 42, 6873–6883,  
1079 2008a.
- 1080 Geng, F. H., Zhang, Q., Tie, X., Huang, M., Ma, X., Deng, Z., Quan, J., and Zhao, C.: Aircraft  
1081 measurements of O<sub>3</sub>, NO<sub>x</sub>, CO, VOCs, and SO<sub>2</sub> in the Yangtze River Delta region, *Atmospheric*  
1082 *Environment*, 43, 584–593, 2008b.
- 1083 Geng, F. H., Tie, X., Guenther, A., Li, G., Cao, J., and Harley, P.: Effect of isoprene emissions from  
1084 major forests on ozone formation in the city of Shanghai, China, *Atmospheric Chemistry and*  
1085 *Physics*, 11, 10449–10459, 2011.
- 1086 Geng, F. H., Mao, X. Q., Zhou, M. Y., Zhong, S. Y., and Lenschow, D.: Multi-year ozone  
1087 concentration and its spectra in Shanghai, China, *Science of the Total Environment*, 521-522,  
1088 135-143, 2015.
- 1089 Gery, M. W., and Crouse, R. R.: *User’s Guide for Executing OZIPR*, Atmospheric Research and  
1090 Exposure Assessment Lab., Office of Research and Development, U.S. EPA, Research Triangle  
1091 Park, N. C., <http://www.epa.gov/scram001/models/other/oziprdme.txt>, 2002.
- 1092 Grell, G. A., Peckham, S. E., Schmitz, R., McKeen, S. A., Frost, G., Skamarock, W. C., and Eder, B.:  
1093 Fully coupled “online” chemistry within the WRF model, *Atmospheric Environment*, 39,  
1094 6957–6975, 2005.
- 1095 Guenther, A., Karl, T., Harley, P., Wiedinmyer, C., Palmer, P. I., and Geron, C.: Estimates of global  
1096 terrestrial isoprene emissions using MEGAN (Model of Emissions of Gases and Aerosols from

---

1097 Nature), Atmospheric Chemistry and Physics, 6, 3181–3210, 2006.

1098 Hong, S. Y. and Lim, J. O. J.: The WRF Single-Moment 6-Class Microphysics Scheme (WSM6),  
1099 Journal of the Korean Meteorological Society, 42, 129–151, 2006.

1100 [Hu, X. M., Klein, P. M., and Xue, M.: Evaluation of the updated YSU planetary boundary layer  
1101 scheme within WRF for wind resource and air quality assessments, Journal of Geophysical  
1102 Research-Atmospheres, 118, 10490-10505, 2013.](#)

1103 [Hu, X. M., Xue, M., Klein, P. M., Illston, B. G., and Chen, S.: Analysis of Urban Effects in Oklahoma  
1104 City using a Dense Surface Observing Network, Journal of Applied Meteorology and  
1105 Climatology, 55, 723-741, 2016.](#)

1106 Lei, W., Foy, B. de, Zavala, M., Volkamer, R., and Molina, L. T.: Characterizing ozone production in  
1107 the Mexico City Metropolitan Area: a case study using a chemical transport model,  
1108 Atmospheric Chemistry and Physics, 7, 1347-1366, 2007.

1109 Li, G., Lei, W., Zavala, M., Volkamer, R., Dusanter, S., Stevens, P., and Molina, L. T.: Impacts of  
1110 HONO sources on the photochemistry in Mexico City during the MCMA-2006/MILAGO  
1111 Campaign, Atmospheric Chemistry and Physics, 10, 6551–6567, 2010.

1112 Li, G., Bei, N., Tie, X., and Molina, L. T.: Aerosol effects on the photochemistry in Mexico City  
1113 during MCMA-2006/MILAGRO campaign, Atmospheric Chemistry and Physics, 11,  
1114 5169–5182, 2011.

1115 Li, K., Jacob, D. J., Liao, H., Shen, L., Zhang, Q., and Bates, K. H.: Anthropogenic drivers of  
1116 2013-2017 trends in summer surface ozone in China, PANS, 116, 2, 422-427, 2019.

1117 Lin, X., Trainer, M., and Liu, S. C.: On the nonlinearity of the tropospheric ozone production,  
1118 Journal of Geophysical Research Atmospheres, 93 (D12), 15879–15888, 1988.

1119 Lin, Y. F., Wang, Q., Fu, Q. Y., Duan, Y. S., Xu, J. M., Liu, Q. Z., Li, F., and Huang, K.: Temporal-spatial  
1120 characteristics and impact factors of ozone pollution in Shanghai, Environmental Monitoring  
1121 in China (in Chinese), 33, 4, 60-67, 2017.

1122 Lin, Y. L., Farley, R. D., and Orville, H. D.: Bulk parameterization of the snowfield in a cloud model,  
1123 Journal of Climate and Applied Meteorology, 22, 1065–1092, 1983.

1124 Lu, X., Hong, J., Zhang, L., Cooper, O., Schultz, M., Xu, X., Wang, T., Gao, M., Zhao, Y., and Zhang, Y.:  
1125 Severe surface ozone pollution in China: A global perspective, Environmental Science  
1126 & Technology Letters, 5, 487–494, 2018.

1127 Monks, P. S., Archibald, A. T., Colette, A., Cooper, O., Coyle, M., Derwent, R., Fowler, D., Granier, C.,  
1128 Law, K. S., Mills, G. E., Stevenson, D. S., Tarasova, O., Thouret, V., von Schneidemesser, E.,  
1129 Sommariva, R., Wild, O., and Williams, M. L.: Tropospheric ozone and its precursors from the  
1130 urban to the global scale from air quality to short-lived climate forcer, Atmospheric  
1131 Chemistry and Physics, 15, 8889–8973, 2015.

1132 Ma, Z., Xu, J., Quan, W., Zhang, Z., Lin, W., and Xu, X.: Significant increase of surface ozone at a  
1133 rural site, north of eastern China, Atmospheric Chemistry and Physics, 16, 3969–3977, 2016.

1134 Nenes, A., Pandis, S. N., and Pilinis, C.: ISORROPIA: A new thermodynamic equilibrium model for  
1135 multiphase multicomponent inorganic aerosols, Aquatic Geochemistry, 4, 123–152, 1998.

1136 Ran, L., Zhao, C., Geng, F., Tie, X., Tang, X., Peng, L., Zhou, G., Yu, Q., Xu, J., and Guenther, A.:  
1137 Ozone photochemical production in urban Shanghai, China: analysis based on ground level  
1138 observations, Journal of Geophysical Research Atmospheres, 114, D15301, 2009.

1139 Sillman, S.: The use of NO<sub>y</sub>, H<sub>2</sub>O<sub>2</sub>, and HNO<sub>3</sub> as indicators for ozone-NO<sub>x</sub>-hydrocarbon sensitivity  
1140 in urban locations, Journal of Geophysical Research Atmospheres, 100, 14175–14188, 1995.

---

1141 Sillman, S.: The relation between ozone, NO<sub>x</sub> and hydrocarbons in urban and polluted rural  
1142 environments, *Atmospheric Environment*, 33, 1821–1845, 1999.

1143 Song, J., Lei, W., Bai, N., Zavala, M., de Foy, B., Volkamer, R., Cardenas, B., Zheng, J., Zhang, R., and  
1144 Molina L. T.: Ozone response to emission changes: a modeling study during the  
1145 MCMA-2006/MILAGRO Campaign, *Atmospheric Chemistry and Physics*, 10, 3827–3846, 2010

1146 Stockwell, W. R., Middleton, P., Chang, J. S., and Tang, X.: The second generation regional acid  
1147 deposition model chemical mechanism for regional air quality modeling, *Journal of*  
1148 *Geophysical Research Atmospheres*, 95, 16343–16367, 1990.

1149 Sun, L., Xue, L., Wang, T., Gao, J., Ding, A., Copper, O., Lin, M., Xu, P., Wang, Z., Wang, X., Wen, L.,  
1150 Zhu, Y., Chen, T., Yang, L., Wang, Y., Chen, J., and Wang, W.: Significant increase of  
1151 summertime ozone at Mount Tai in central eastern China, *Atmospheric Chemistry and*  
1152 *Physics*, 16, 10637–10650, 2016.

1153 Tai, A. P. K., Martin, M. V., and Heald, C. L.: Threat to future global food security from climate  
1154 change and ozone air pollution, *Nature Climate Chang*, 4, 817–821, 2014.

1155 Tang, G., Li, X., Wang, Y., Xin, J., and Ren, X.: Surface ozone trend details and interpretations in  
1156 Beijing, 2001–2006, *Atmospheric Chemistry and Physics*, 9, 8813–8823, 2009.

1157 Tang, W. Y., Zhao, C. S., Geng, F. H., Peng, L., Zhou, G. Q., Gao, W., Xu, J. M., and Tie, X. X.: Study of  
1158 ozone "weekend effect" in Shanghai, *Science in China Series D: Earth Sciences*, 51, 9,  
1159 1354–1360, 2008.

1160 Tie, X., Brasseur, G., Emmons, L., Horowitz, I., and Kinnison, D.: Effects of aerosols on  
1161 tropospheric oxidants: a global model study, *Journal of Geophysical Research Atmospheres*,  
1162 106, 22931–22964, 2001.

1163 Tie, X., Madronich, S., Walters, S., Zhang, R. Y., Rasch, P., and Collins, W.: Effect of clouds on  
1164 photolysis and oxidants in the troposphere, *Journal of Geophysical Research Atmospheres*,  
1165 108, 4642, doi:10.1029/2003jd003659, 2003.

1166 Tie, X., Madronich, S., Li, G., Ying, Z., Zhang, R., Garcia, A., Taylor, J., and Liu, Y.: Characterizations  
1167 of chemical oxidants in Mexico City: A regional chemical dynamical model (WRF-Chem)  
1168 study, *Atmospheric Environment*, 41, 1989–2008, 2007.

1169 Tie, X., Geng, F. H., Peng, L., Gao, W., Zhao, C. S.: Measurement and modeling of O<sub>3</sub> variability in  
1170 Shanghai, China: application of the WRF-Chem model, *Atmospheric Environment*, 43,  
1171 4289–4302, 2009a.

1172 Tie, X., Madronich, S., Li, G., Ying, Z., Weinheimer, A., Apel, E., and Campos, T.: Simulation of  
1173 Mexico City plumes during the MIRAGE-Mex field campaign using the WRF-Chem model,  
1174 *Atmospheric Chemistry and Physics*, 9, 4621–4638, 2009b.

1175 Tie, X., Geng, F., Guenther, A., Cao, J., Greenberg, J., Zhang, R., Apel, E., Li, G., Weinheimer, A.,  
1176 Chen, J., and Cai, C.: Megacity impacts on regional ozone formation: observations and  
1177 WRF-Chem modeling for the MIRAGE-Shanghai field campaign, *Atmospheric Chemistry and*  
1178 *Physics*, 13, 5655–5669, doi:10.5194/acp-13-5655-2013, 2013.

1179 Wang, H. J., and Chen, H. P.: Understanding the recent trend of haze pollution in eastern China:  
1180 roles of climate change, *Atmospheric Chemistry and Physics*, 16, 4205–4211, 2016

1181 Wang, T., Xue, L., Brimblecombe, P., Lam Y. F., Li, L., and Zhang, L.: Ozone pollution in China: A  
1182 review of concentrations, meteorological influences, chemical precursors, and effects,  
1183 *Science of Total Environment*, 575, 1582–1596, 2017.

1184 Wesely, M. L.: Parameterization of surface resistances to gaseous dry deposition in regional-scale

---

1185 numerical models, *Atmospheric Environment*, 23, 1293–1304, 1989.

1186 Xu, J. M., Yan, F. X., Xie, Y., Wang, F. Y., Wu, J. B., and Fu, Q. Y.: Impact of meteorological conditions  
1187 on a nine-day particulate matter pollution event observed in December 2013, Shanghai,  
1188 China, *Particuology*, 20, 69–79, 2015.

1189 Xu, J. M., Chang, L. Y., Yan, F. X., and He, J. H.: Role of climate anomalies on decadal variation in  
1190 the occurrence of wintertime haze in the Yangtze River Delta, China, *Science of the Total  
1191 Environment*, 599-600, 918-925, 2017.

1192 Ying, Z. M., Tie, X., and Li, G. H.: Sensitivity of ozone concentrations to diurnal variations of  
1193 surface emissions in Mexico City: A WRF/Chem modeling study, *Atmospheric Environment*,  
1194 43, 851–859, 2009.

1195 Zhang, Q., Streets, D. G., Carmichael, G. R., He, K. B., Huo, H., Kannari, A., Klimont, Z., Park, I. S.,  
1196 Reddy, S., Fu, J. S., Chen, D., Duan, L., Lei, Y., Wang, L. T., Yao, Z. L.: Asian emissions in 2006  
1197 for the NASA INTEX-B mission, *Atmospheric Chemistry and Physics*, 9, 5131-5153, 2009.

1198 Zhao, S., Li, J. P., Sun, C.: Decadal variability in the occurrence of wintertime haze in central  
1199 eastern China tied to the Pacific decadal oscillation, *Scientific Reports*, 6, 27424, 2016.

1200 Zheng, B., Tong, D., Li, M., Liu, F., Hong, C., Geng, G., Li, H., Li, X., Peng, L., Qi, J., Yan, L., Zhang, Y.,  
1201 Zhao, H., Zheng, Y., He, K., and Zhang, Q.: Trends in China's anthropogenic emissions since  
1202 2010 as the consequence of clean air actions, *Atmospheric Chemistry and Physics*, 18,  
1203 14095-14111, <https://doi.org/10.5194/acp-18-14095-2018>, 2018.

1204 Zhou, G. Q., Xu, J. M., Xie, Y., Chang, L. Y., and Gao, W.: Numerical air quality forecasting over  
1205 eastern China: An operational application of WRF-Chem, *Atmospheric Environment*, 153,  
1206 94-108, 2017.

1207



1208 **Table 1.** Statistical analysis on O<sub>3</sub> simulation in September of 2009 by WRF-Chem model  
 1209 compared with measurements of 5 sites (XJH, JS, DT, PD, BS) over Shanghai. MO and MM  
 1210 represent the mean value (unit: ppbv) of observed and modeled O<sub>3</sub> concentration respectively.  
 1211 RMSE and R are the Root Mean Square Error and correlated coefficient respectively calculated  
 1212 between modeled and measured O<sub>3</sub> concentration.  
 1213

	MO	MM	RMSE	R (99% confidence)
		ppbv		\
<b>XJH</b>	21.6	23.0	7.2	0.78
<b>JS</b>	34.6	30.0	10.3	0.64
<b>DT</b>	47.3	40.3	12.0	0.61
<b>PD</b>	33.5	34.9	8.6	0.74
<b>BS</b>	31.7	31.2	9.3	0.67

1214  
 1215  
 1216  
 1217 **Table 2.** Statistical analysis on NO<sub>x</sub> simulation in September of 2009 by WRF-Chem model  
 1218 compared with measurements of 5 sites (XJH, JS, DT, PD, BS) over Shanghai. MO and MM  
 1219 represent the mean value (unit: ppbv) of observed and modeled NO<sub>x</sub> concentration respectively.  
 1220 RMSE and R are the Root Mean Square Error and correlated coefficient respectively calculated  
 1221 between modeled and measured NO<sub>x</sub> concentration.  
 1222

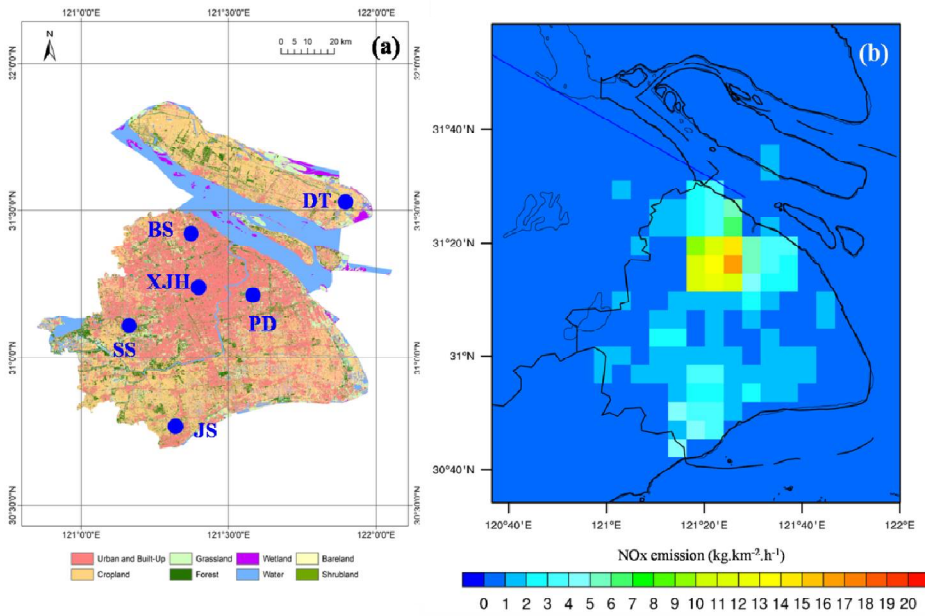
	MO	MM	RMSE	R (99% confidence)
		ppbv		\
<b>XJH</b>	32.1	33.7	7.0	0.74
<b>JS</b>	14.9	14.7	7.6	0.61
<b>DT</b>	3.0	1.5	2.3	0.6
<b>PD</b>	20.3	16.8	7.5	0.82
<b>BS</b>	21.6	16.1	9.8	0.8

1223  
 1224  
 1225 **Table 3.** Scheme of WRF-Chem sensitivity simulations.  
 1226

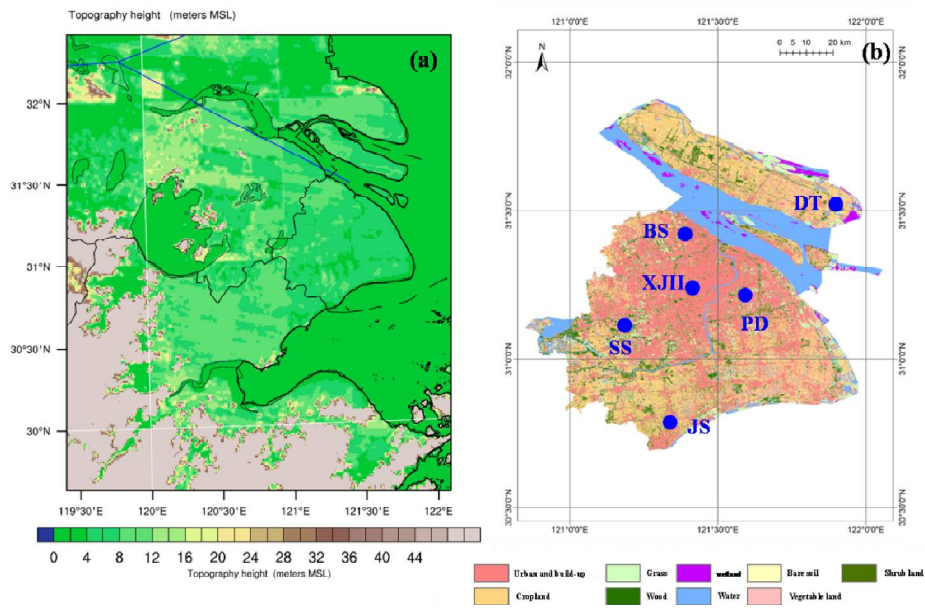
Simulation	NO <sub>x</sub> EI	VOCs EI	Meteorology
<b>T1 (Control Run)</b>	2009	2009	September of 2009
<b>T2</b>	2015 (30% reduction)	2009	September of 2009
<b>T3</b>	2009	50% increasing	September of 2009
<b>T4</b>	2020 (50% reduction)	2009	September of 2009
<b>T5</b>	2015	50% increasing	September of 2009
<b>T6</b>	70% reduction	2009	September of 2009
<b>T7</b>	2020 (50% reduction)	50% increasing	September of 2009

1227  
 1228  
 1229

1230



1231



1232

1233

1234

1235

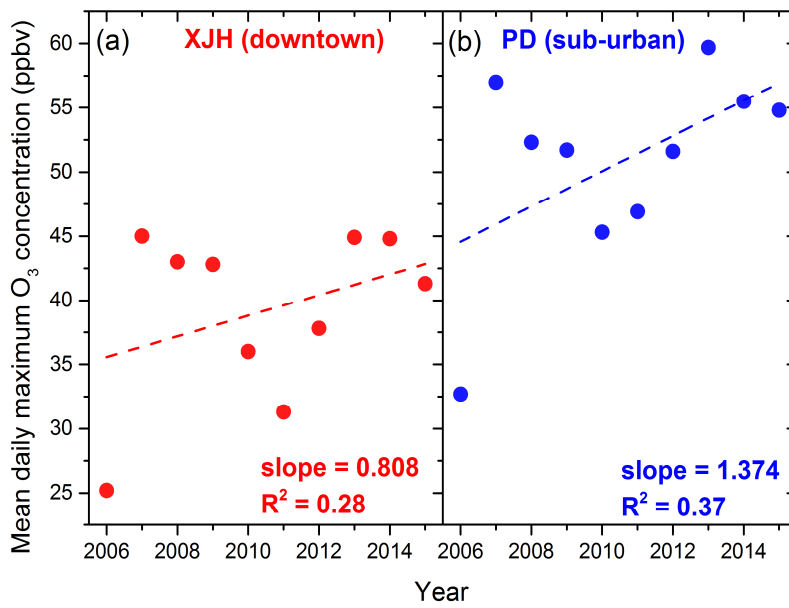
1236

1237

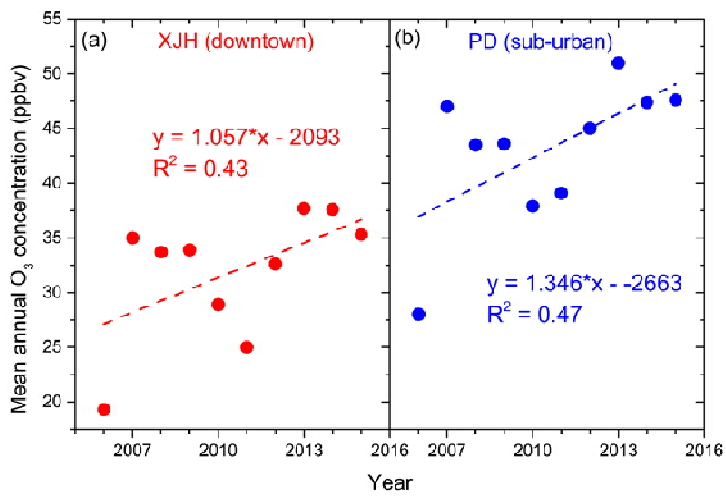
1238

**Figure1** (a) The distribution of land-use category in Shanghai. The blue dots denote the locations of 6 sties (XJH, BS, PD, SS, JS, DT). (b) The NOx emission of 2009 scenario in Shanghai. **Figure 1. (a)** The distribution of topography height in Shanghai and its neighboring area. (b) The distribution of land-use category in Shanghai. The locations of the 6 sites (XJH, BS, PD, SS, JS, DT) are described by blue dots.

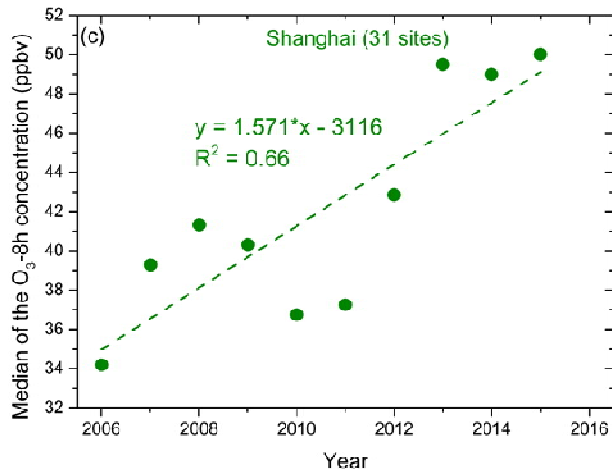
带格式的：字体：非加粗



1239

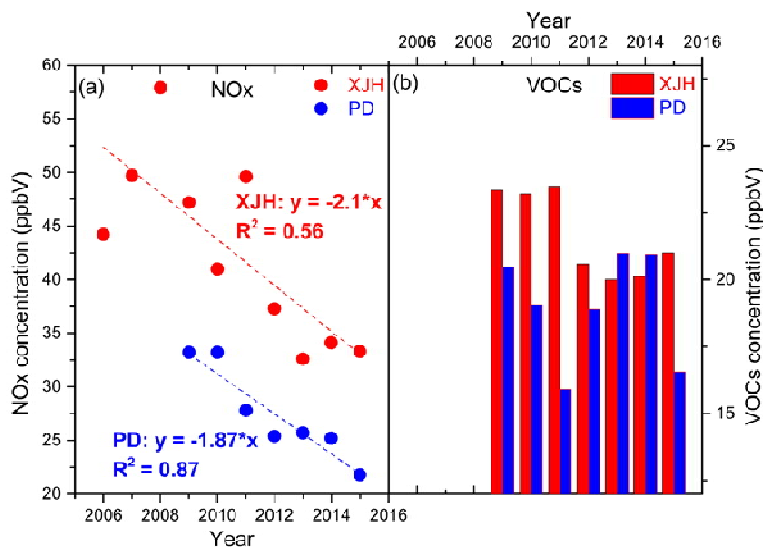


1240



1241

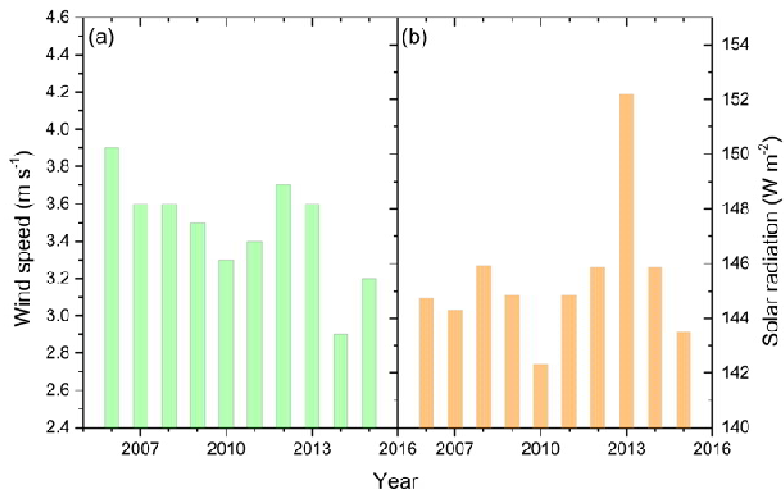
1242 **Figure 2.** The ~~mean~~ annual variation of daily maximum O<sub>3</sub> concentration (ppbv) from 2006 to  
 1243 2015 at (a) downtown site XJH and (b) sub-urban site PD, both presenting the significant  
 1244 increasing trends with 1.0570.808 ppbv yr<sup>-1</sup> at XJH and 1.3461.374 ppbv yr<sup>-1</sup> at PD. The variation  
 1245 of the median 8-h O<sub>3</sub> concentration (ppbv) from 2006 to 2015 averaged for 31 sites over  
 1246 Shanghai (c), also shows the increasing variability of 1.571 ppbv yr<sup>-1</sup>.



1247

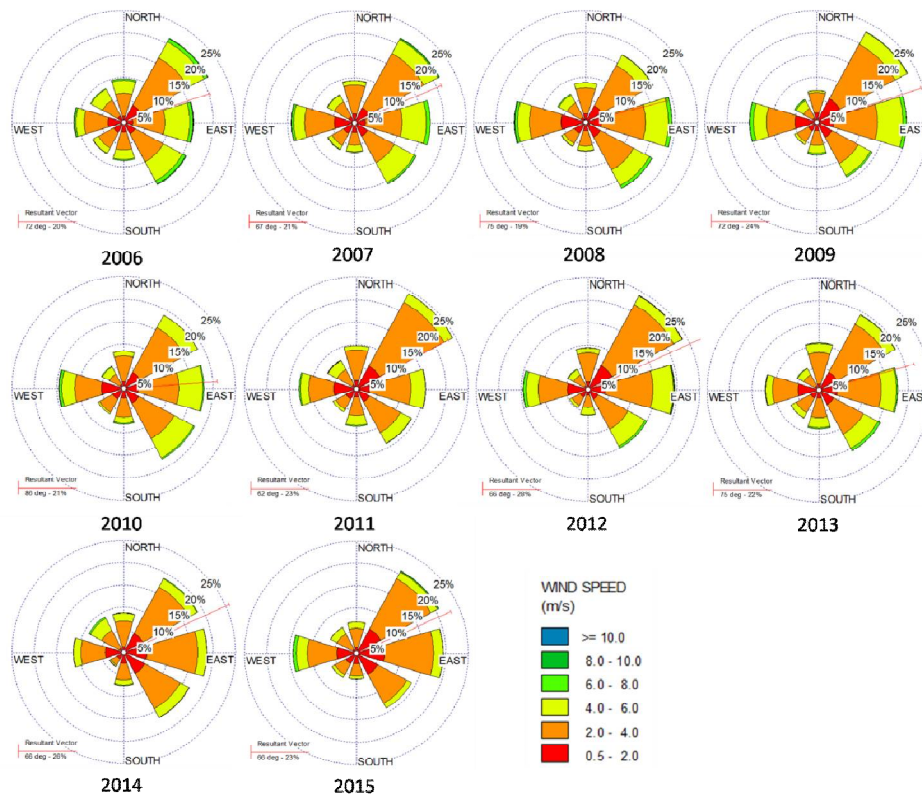
1248 **Figure 3.** The mean annual concentrations (ppbv) of (a) NO<sub>x</sub> (dots) and (b) VOCs (bars) from 2006  
 1249 to 2015 at downtown site XJH and sub-urban site PD respectively. The NO<sub>x</sub> concentrations at XJH  
 1250 and PD both present obvious decreasing trends with 2.1 ppbv yr<sup>-1</sup> and 1.87 ppbv yr<sup>-1</sup>. While the  
 1251 VOCs concentrations at both sites present no clear inter-annual trends.

1252



1253  
 1254  
 1255  
 1256  
 1257  
 1258  
 1259

**Figure 4.** The annual variation of (a) summer wind speed ( $\text{m s}^{-1}$ ) and (b) total solar radiation ( $\text{W m}^{-2}$ ) from 2006 to 2015 in Shanghai. Both wind speed and the solar radiation present weak inter-annual variations but without significant trends.



1260

1261

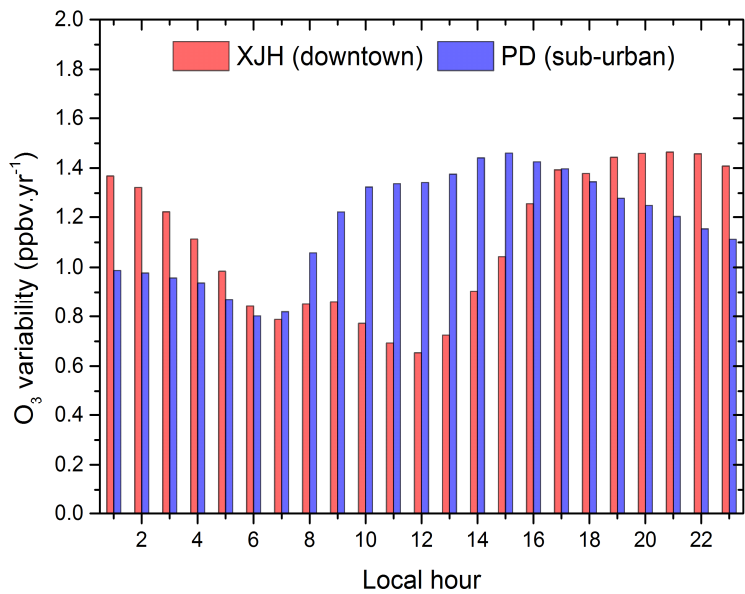
**Figure 5.** The wind rose of each year from 2006 to 2015 in Shanghai. The red line means the resultant vector suggesting the dominant wind direction.

1262

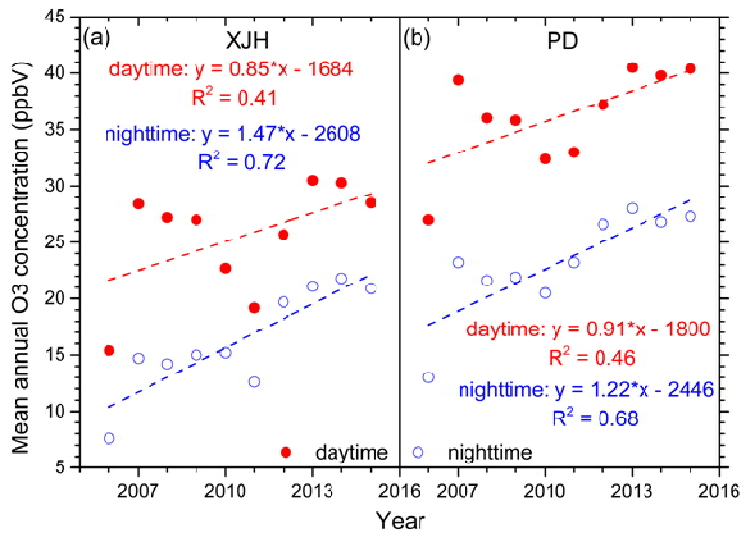
1263

1264

1265



1266

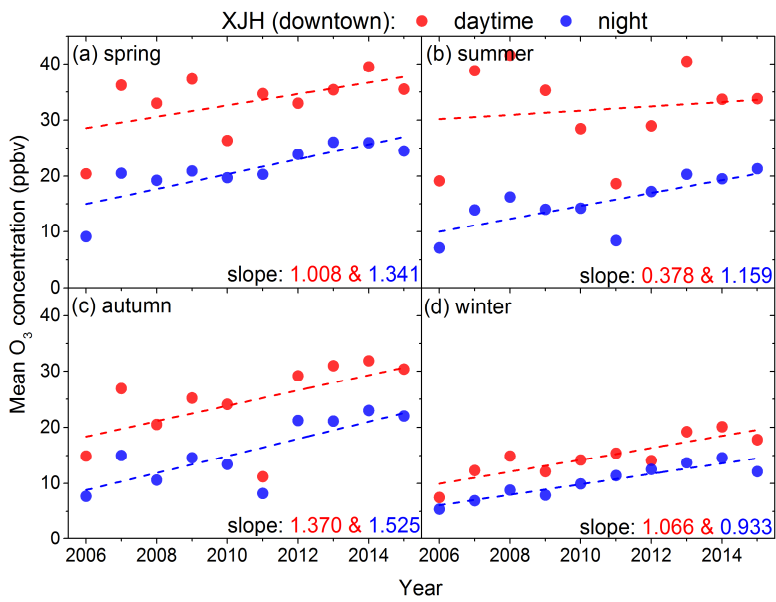


1267

1268 **Figure 6. The variability of hourly O<sub>3</sub> concentration from 2006 to 2015 at downtown site XJH (red**  
 1269 **bars) and sub-urban site PD (blue bars).The annual variations of daytime and nighttime O<sub>3</sub>**  
 1270 **concentration (ppbv) from 2006 to 2015 at (a) downtown site XJH and (b) sub-urban site PD.**

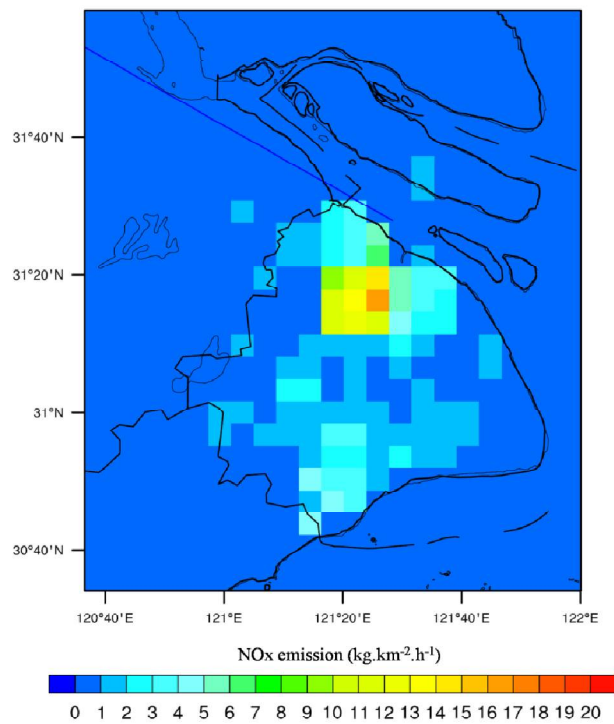
1271

带格式的：下标



1272  
1273  
1274  
1275

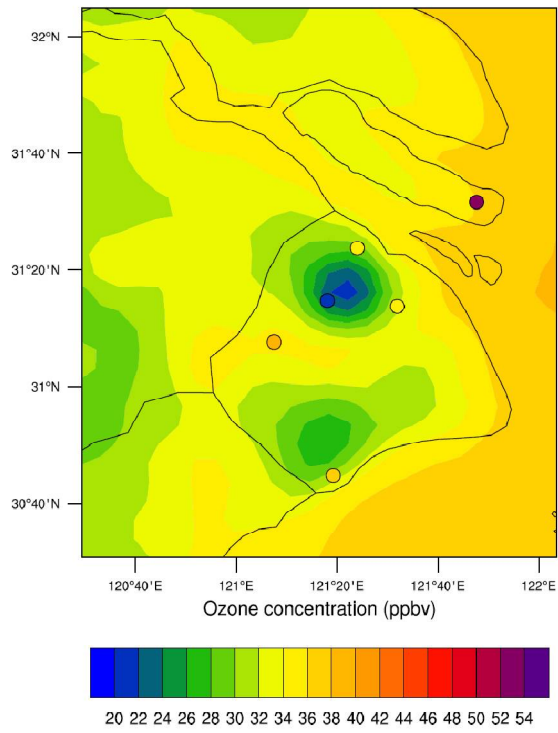
**Figure 7.** The daytime (8:00-18:00, BJT) and nighttime (19:00-07:00, BJT) O<sub>3</sub> variability from 2006 to 2015 at downtown site XJH in (a) spring, (b) summer, (c) autumn and (d) winter.



1276  
1277

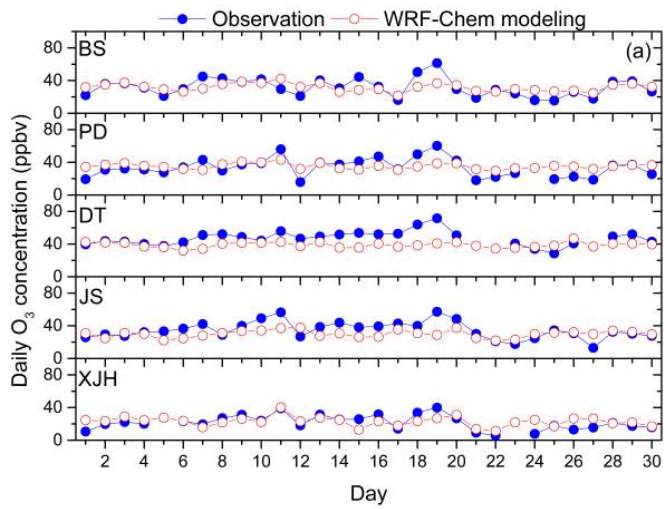
**Figure 7.** The distribution of NO<sub>x</sub> emission ( $\text{kg km}^{-2} \text{h}^{-1}$ ) in 2009 in Shanghai.



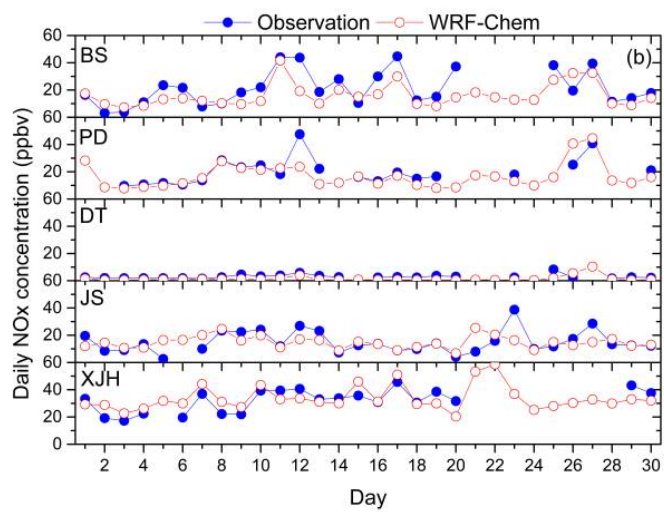


1278  
1279  
1280  
1281

**Figure 8.** The calculated distribution of O<sub>3</sub> concentration by WRF-Chem (shade) in September of 2009 compared with measurements (circles) of 6 sites over Shanghai.



1282



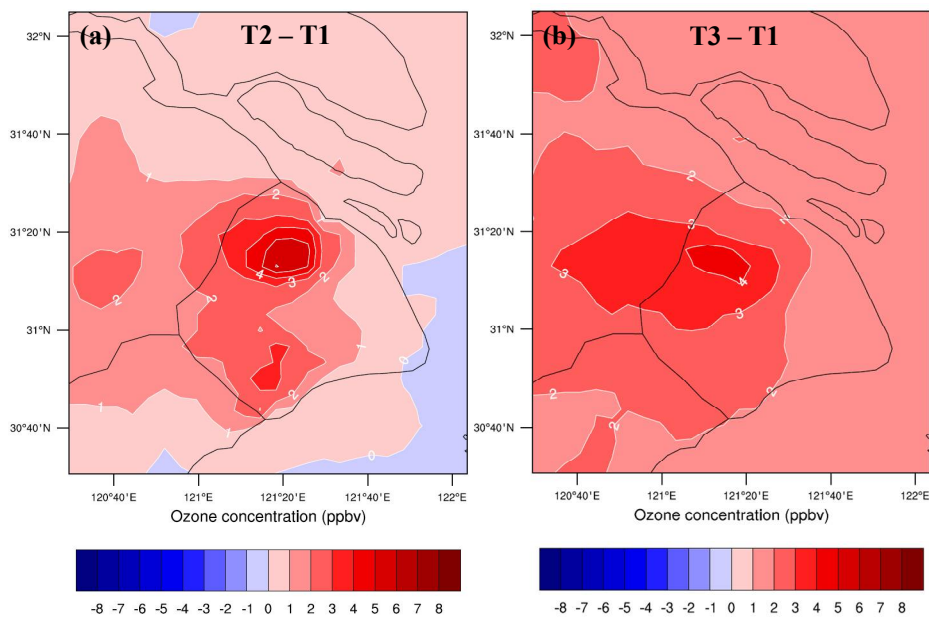
1283

1284

**Figure 9.** The calculated mean daily concentrations (ppbv) of (a)  $O_3$  and (b)  $NO_x$  at 5 sites in September of 2009 by WRF-Chem (red circles) and compared with measurements (blue circles).

1285

1286



1287

1288

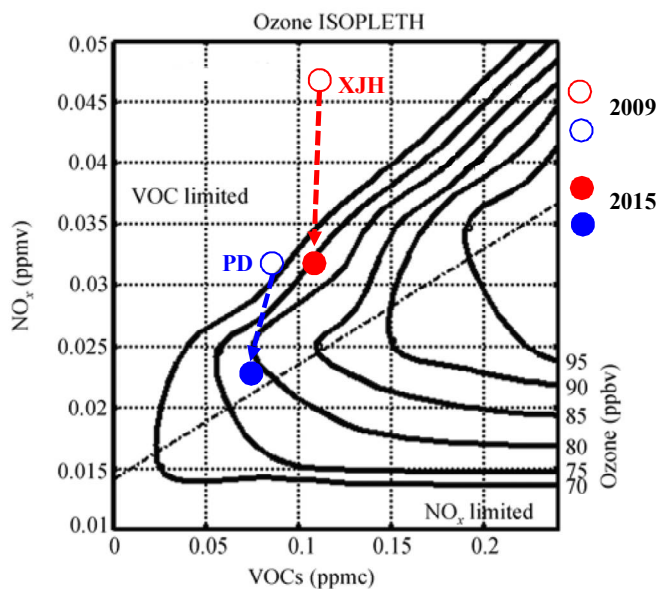
1289

1290

1291

1292

**Figure 10.** The difference of O<sub>3</sub> concentration (ppbv) between (a) T2 and T1 (T2-T1), (b) T3 and T1 (T3-T1) respectively conducted by WRF-Chem model. The difference between T2 and T1 lies in the NO<sub>x</sub> emissions set in T2 (2015 scenario) is 30% lower than that in T1 (2009 scenario), which is estimated by Lin et al. (2017) according to the Shanghai Environment Yearbook. The difference between T3 and T1 is dependent on that the VOCs emission in T3 is 50% higher than that in T1.



1293

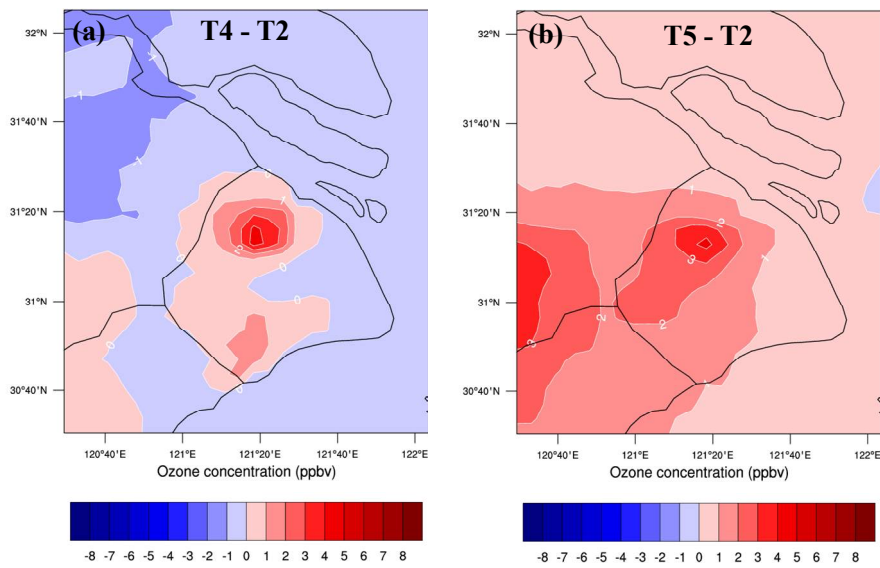
1294

1295

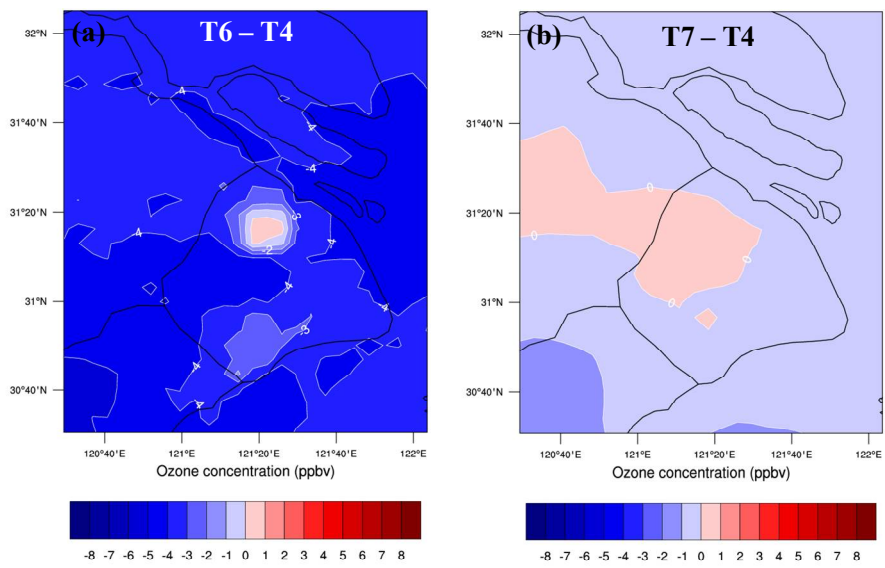
1296

1297

**Figure 11.** The O<sub>3</sub> chemical production at downtown site XJH and sub-urban site PD in 2009 and 2015 depicted by O<sub>3</sub> isopleths diagram. The hollow and solid red circles denote O<sub>3</sub> production regime at XJH in 2009 and 2015 respectively. The hollow and solid blue circles denote O<sub>3</sub> production regime at PD in 2009 and 2015 respectively



1298  
 1299 **Figure 12.** The difference of O<sub>3</sub> concentration (ppbv) between (a) T4 and T2 (T4-T2), (b) T5 and  
 1300 T2 (T5-T2) respectively conducted by WRF-Chem model. The difference between T4 and T2 is  
 1301 that the NO<sub>x</sub> emissions set in T4 (2020 scenario) is 20% lower than that in T2 (2015 scenario),  
 1302 which is estimated according to the Shanghai Clean Air Action Plan. The difference between T5  
 1303 and T2 lies in that the VOCs emission in T5 is 50% higher than that in T2.  
 1304  
 1305  
 1306  
 1307



1308  
 1309 **Figure 13.** The difference of O<sub>3</sub> concentration (ppbv) between (a) T6 and T4 (T6-T4), (b) T7 and  
 1310 T4 (T7-T4) respectively conducted by WRF-Chem model. The NO<sub>x</sub> emissions set in T6 is 20% lower  
 1311 than that in T4 (2020 scenario). The VOCs emission in T7 is 50% higher than that in T4.